JACS
JOURNAL OF THE AMERICAN CHEMICAL SOCIETY

ARTICLE

pubs.acs.org/JACS

Explanation for Main Features of Structure−Genotoxicity Relationships of Aromatic Amines by Theoretical Studies of Their Activation Pathways in CYP1A2

Igor Shamovsky,*[,†] Lena Ripa,[†] Lena Börjesson,[†] Christine Mee,[‡] Bo Nordén,[†] Peter Hansen,[†] Catrin Hasselgren,[§] Mike O'Donovan,[‡] and Peter Sjö[†]

[†]Department of Medicinal Chemistry, R&I iMed, AstraZeneca R&D, Pepparedsleden 1, S-431 83 Mölndal, Sweden

[‡]Genetic Toxicology, AstraZeneca R&D, Alderley Park, Macclesfield, Cheshire SK10 4TG, United Kingdom

[§]Global Safety Assessment, AstraZeneca R&D, S-431 83 Mölndal, Sweden

Supporting Information

ABSTRACT: Aromatic and heteroaromatic amines ($ArNH_2$) represent a class of potential mutagens that after being metabolically activated covalently modify DNA. Activation of $ArNH_2$ in many cases starts with *N*-hydroxylation by P450 enzymes, primarily CYP1A2. Poor understanding of structure−mutagenicity relationships of $ArNH_2$ limits their use in drug discovery programs. Key factors that facilitate activation of $ArNH_2$ are revealed by exploring their reaction intermediates in CYP1A2 using DFT calculations. On the basis of these calculations and extensive analysis of structure−mutagenicity data, we suggest that mutagenic metabolites are generated by ferric peroxo intermediate, $(CYP1A2)Fe^{III}-OO^-$, in a three-step heterolytic mechanism. First, the distal oxygen of the oxidant abstracts proton from H-bonded $ArNH_2$. The subsequent proximal protonation of the resulting $(CYP1A2)Fe^{III}-OOH$ weakens both the O−O and the O−H bonds of the oxidant. Heterolytic cleavage of the O−O bond leads to *N*-hydroxylation of $ArNH^-$ via S_N2 mechanism, whereas cleavage of the O−H bond results in release of hydroperoxy radical. Thus, our proposed reaction offers a mechanistic explanation for previous observations that metabolism of aromatic amines could cause oxidative stress. The primary drivers for mutagenic potency of $ArNH_2$ are (i) binding affinity of $ArNH_2$ in the productive binding mode within the CYP1A2 substrate cavity, (ii) resonance stabilization of the anionic forms of $ArNH_2$, and (iii) exothermicity of proton-assisted heterolytic cleavage of N−O bonds of hydroxylamines and their bioconjugates. This leads to a strategy for designing mutagenicity free $ArNH_2$: Structural alterations in $ArNH_2$, which disrupt geometric compatibility with CYP1A2, hinder proton abstraction, or strongly destabilize the nitrenium ion, in this order of priority, prevent genotoxicity.

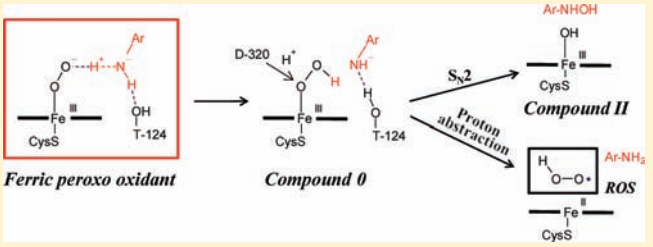

INTRODUCTION

Aromatic and heteroaromatic amines ($ArNH_2$) represent convenient building blocks in drug discovery programs because of their synthetic feasibility, valuable physicochemical properties, and potential for specific interactions with binding sites of target proteins. However, concerns over mutagenic and carcinogenic potential restrict their wide use as pharmaceutical building blocks. Nevertheless, a small number of marketed drugs that are free of mutagenicity contain $ArNH_2$ fragments linked through carboxamide or sulphonamide bonds, for example, atorvastatin.[1,2] Because aromatic amine fragments of drugs could be released by metabolism of such amides, one has to make sure that the entire molecule as well as potential $ArNH_2$ fragments are free of mutagenicity.[3] According to the AstraZeneca in-house Ames mutagenicity database, only 29% of primary $ArNH_2$ tested are bacterial mutagens. This indicates that a wider use of $ArNH_2$ in drug discovery programs might be possible, provided a rational design strategy for prevention of genotoxicity in $ArNH_2$, based on mechanistic understanding of the origin of the observed structure−mutagenicity relationships, is developed. If the actual mechanism of metabolic activation of $ArNH_2$ is identified, this would enable us to find ways to hinder particular chemical events that lead to formation of mutagenic products.

Interest in the carcinogenicity of $ArNH_2$ started over 100 years ago when it was realized that urinary bladder cancer in men was associated with occupational exposure to anilines in the dye industry.[4−6] Since then, significant efforts have been devoted to investigate their impact on human health resulting from environmental contaminants, dietary components, and smoking, and to understand the mechanisms underlying their ability to induce cancer in man and experimental animals. Many mutagenic and carcinogenic $ArNH_2$ are currently widely present in our environment.[6−13] Aromatic and heteroaromatic amines, like many carcinogens, become mutagenic only after metabolic transformation by a series of reactions.[6,7,14−22] Metabolic activation of $ArNH_2$ in most cases starts with *N*-hydroxylation by the 1A subfamily of

Received: July 11, 2011
Published: September 06, 2011

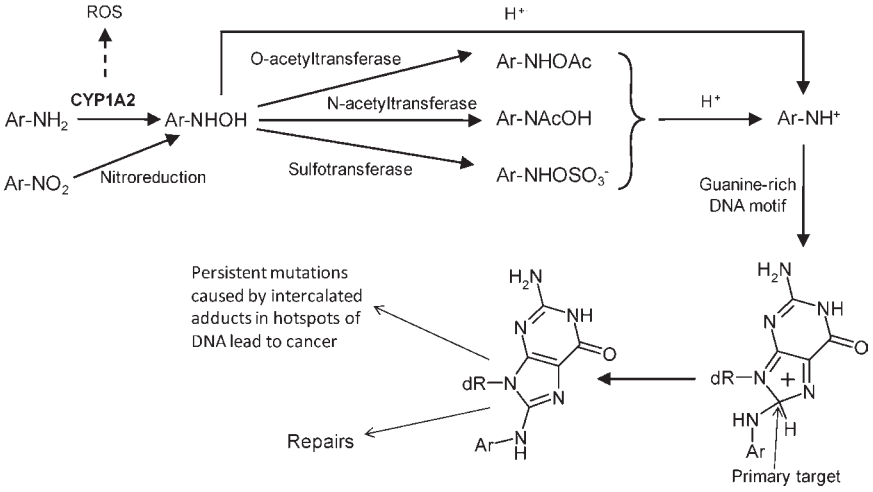

Figure 1. Two mutagenic pathways of aromatic amines induced by interactions with CYP1A2. The major route, through *N*-hydroxylation to hydroxylamines and nitrenium ions, results in covalent adducts with DNA guanines. The second route is through generation of ROS and oxidative stress. Nitroarenes follow the same pathway toward the DNA adducts after nitroreduction by bacterial nitroreductase to hydroxylamines. Heterolytic dissociation of hydroxylamines and their esters to nitrenium ions is catalyzed by protonation under acidic conditions.[31,108]

cytochrome P450 enzymes (Figure 1), primarily by CYP1A2 and, to a lesser extent, by CYP1A1.[6,21−25] Hydrolytic dissociation of the resulting hydroxylamines may directly lead to nitrenium ions, the postulated ultimate reactive electrophilic species that covalently modify nucleic bases of DNA.[6,22] Alternatively, hydroxylamines may get further metabolized by Phase II enzymes, such as *N*-acetyl-, sulfo- and UDP glucoronosyl-transferases, prolyl tRNA synthetase, and kinases, leading to even more reactive bioconjugates,[6,15,22−30] which eventually also result in nitrenium ions.[21,22,31]

Replication of covalent DNA adducts results in frameshift mutations,[11,27,32] with persistent mutations in DNA hotspots being able to cause cancer.[27,29] Because there are many enzymes, activation steps, and factors involved in mutagenesis and carcinogenesis of $ArNH_2$,[11,13,17,29,32−38] the resulting structure−mutagenicity relationships are poorly understood.[3,10,17,39] The C8 position of guanine residues of DNA is known to be the primary target for covalent modifications;[14,40] however, particular nitrenium ions may also react with other guanine atoms or other DNA bases,[6,28,29,32,41] which further complicates the structure−mutagenicity relationships. In addition to the formation of pro-mutagenic $ArNH_2$−DNA adducts, it has been suggested that interaction of a number of $ArNH_2$ with P450 enzymes and peroxidases caused formation of reactive oxygen species (ROS) and induced lipid peroxidation, which may also lead to mutations in DNA and cancer (Figure 1).[42−47]

Structure−mutagenicity relationships of $ArNH_2$ have been a subject of extensive research for decades.[10,13,29,39,48−57] In earlier publications, stability of nitrenium ions was found to correlate with the mutagenic potency of $ArNH_2$.[50,58−60] However, the role of nitrenium ion stability in mutagenic potency of $ArNH_2$ remains disputed because of later findings that suggest that addition of electron-withdrawing groups, which destabilize nitrenium ions, increase mutagenicity in various classes of $ArNH_2$.[13,29,39,61] Multivariate studies showed that the electron affinity of the parent $ArNH_2$ measured as the inverse energy of the lowest unoccupied molecular orbital, LUMO, is the dominant predictor of mutagenic potency of $ArNH_2$ in addition to the size of the aromatic π-electron system.[13,39,52] The chemical grounds of such findings

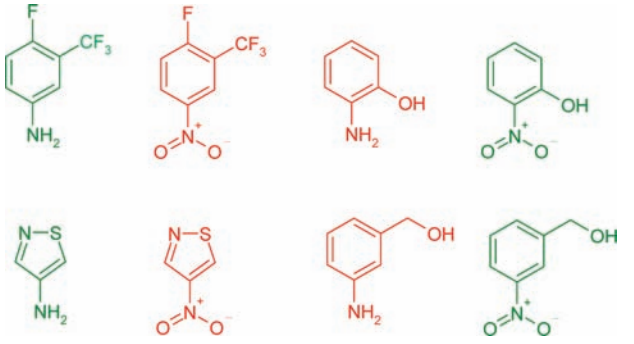

Figure 2. Difference in Ames mutagenicity of aromatic amines and the corresponding nitroarenes in TA98/TA100 strains (mutagenic compounds are shown in red, while mutagenicity-free compounds are in green).

are unknown.[13,39] However, at this point, it becomes clear that the nitrenium stabilization concept ignores an important factor that allows electron-withdrawing functions to increase mutagenic potency of $ArNH_2$. Thus, data reported by Borosky suggest that nitrenium ion stability does not explain the structure−mutagenicity relationship of aromatic and heteroaromatic $ArNH_2$ of different sizes.[60] Consistent with previous studies,[33,61] it was shown that the presence of electronegative pyridine-like nitrogens split the overall structure−mutagenicity relationship into several subclasses, and within each of these subclasses the structure−mutagenicity relationship was dominated by the effect of the size of the aromatic system. Another indication of a secondary role that nitrenium ion stability plays in the mutagenic potency of $ArNH_2$ is the difference in mutagenicity of $ArNH_2$ and that of the corresponding nitroarenes, in which NO_2 replaces NH_2.[53] These classes are metabolized by different enzymes but through identical hydroxylamines (Figure 1);[2,62,63] therefore, the difference in their mutagenicity (e.g., see Figure 2) cannot be caused by different stabilities of nitrenium ions or by any other event that follows the formation of hydroxylamines. These data strongly suggest that the lack of mutagenicity of 4-fluoro-3-trifluoromethylaniline and 1,2-thiazol-4-amine in Figure 2 is because of inability of CYP1A2 to form hydroxylamines from them. Lack of

understanding of the underlying drivers of the observed structure−mutagenicity relationships of $ArNH_2$ implies that the nature of the mutagenic potency-determining chemical events in the mutagenicity pathway of $ArNH_2$ is not yet identified.[39]

The missing chemical events in the mutagenic pathways that would explain the key features of structure−mutagenicity relationships of $ArNH_2$ are likely to be in the course of N-hydroxylation of $ArNH_2$ by P450 enzymes.[39,64] Most publications suggest a neutral aminyl radical as a key reaction intermediate in the *N*-hydroxylation pathway, in line with the "H abstraction−O rebound" mechanism, which has been established for *C*-hydroxylation by P450 enzymes.[57,65−68] Other publications hypothesized cation-radicaloid or nitrenium forms.[19,43,64] None of these species depends on the direct involvement of LUMO of $ArNH_2$ or could explain the pro-mutagenic effects of electron-withdrawing groups.[13,39] On the other hand, the ability of $ArNH_2$ to generate oxidative stress upon binding to CYP1A2 (Figure 1) increases with stabilization of cationic forms, as it is increased not by electron-withdrawing but by π-electron-donating groups in resonance positions.[43]

A number of QSAR modeling approaches and expert systems have been used to predict mutagenicity of $ArNH_2$.[3,69,70] Many of these are commercial software; their predictive power can approach the experimental reproducibility of Ames tests of organic compounds in different laboratories, although depending on the data set used to assess performance.[70,71] The predictivity also varies between different chemical classes, and the mutagenicity of $ArNH_2$ remains especially difficult to predict.[3] This is not really surprising as mutagenicity of $ArNH_2$ is affected by very slight changes in substituents or substitution patterns,[10,17,39] and QSAR models tend to be too insensitive to capture the effects of such slight changes. Besides, predictive Ames mutagenicity models based on different combinations of chemical descriptors and machine learning techniques do not provide us with an understanding of the origin of the observed structure−mutagenicity relationships.

The purpose of this study was to find out the chemical origin of the observed structure−activity relationships of $ArNH_2$ inherent in the mutagenic pathways in CYP1A2. We investigate activation pathways of a series of para-substituted anilines and 2-aminopyridines in CYP1A2 on the basis of SAR analysis and quantum chemical calculations. Our results suggest a novel heterolytic mechanism involving an initial proton abstraction from the H-bonded arylic amino group to generate an anionic intermediate. We also propose that, depending on the stability of the anionic intermediate, metabolic activation of $ArNH_2$ can proceed to either *N*-hydroxylation or release of a hydroperoxy radical. The results enable us to rationalize the SAR of the compounds under study and $ArNH_2$ in a broader context and provide a rational basis for prediction of mutagenicity of $ArNH_2$ through understanding of the metabolic activation process.

METHODS

DFT Calculations. Fully optimized Density Functional Theory (DFT) calculations at the B3LYP/6-31G* level of theory[72] were utilized to study energetics of enzymatic reactions of bound aromatic amines in the catalytic center of human cytochrome P450 1A2 (CYP1A2). This particular theoretical approximation has been widely used before to study model iron−porphyrin systems, including catalytic centers of P450 enzymes.[67,73] Double-zeta Chizmadia's effective core potentials CSDZ were used to describe inner orbitals of Fe.[74] In line with previous theoretical studies, the electron structures of complexes of the ferric peroxide intermediate were characterized as dianionic doublet, which after the first protonation event was transferred to anionic doublet.[67] Open-shell systems were treated in the framework of the unrestricted formalism. To find the 3D geometry of the molecular systems under study with the lowest possible energy, their redundant internal coordinates were optimized. Geometric constraints have been applied to ensure relevance of the molecular systems to the CYP1A2 binding site.

The B3LYP/6-31G* approximation is a fast and reliable tool to study large molecular systems, particularly enzymatic sites with transition metals.[75] It should be noted, however, that several deficiencies of the B3LYP functional have been observed.[75] The effects of such deficiencies, most importantly inability to describe attractive intermolecular dispersion interactions, have to be taken into consideration. In addition, the basis set normally has to include diffuse functions to improve description of anionic molecular systems.[76] To evaluate the effects of such deficiencies on the main conclusions of this report, other levels of theory were utilized for selected systems, that is, B3LYP/6-31+G* that contained diffuse functions, M06-2X/6-31+G* that was devised to properly describe dispersion interactions,[77] and benchmark ab initio calculations, such as frozen-core Møller−Plesset second-order perturbation theory MP2/6-311+G* and MP2/6-311++G(2df,2p).[78]

When studying enzymatic reactions within CYP1A2, it is very important to maintain the particular molecular environment inherent in the CYP1A2 catalytic domain, revealed by X-ray crystallographic studies (Figure 3).[79] We choose to use the DFT-only approach, rather than a QM/MM alternative.[67] Accordingly, positions of the residues adjacent to the catalytic center and conformation of the axial catalytic residue Cys-458 with respect to the heme inherent in CYP1A2[79] were maintained by geometric constraints. Residue Cys-458 was replaced by axial methyl−thiolate, CH_3S^-, and the side chains of porphyrin shown by thin lines in Figure 3 were removed. The location of the iron−porphyrin heme model with respect to the entire enzyme was defined by superposition with X-ray coordinates of Cβ and S of Cys-458 and four nitrogens of the porphyrin ring in CYP1A2. Cartesian coordinates of Fe^{III} and the direction of the symmetry axis of the porphyrin ring, as well as the observed conformation of the SCH_3 bond with respect to the porphyrin (nearly eclipsed with one of the Fe−N bonds), were kept fixed during geometry optimizations. Rotation of the porphyrin ring around the axis of symmetry was also prevented by a torsion angle constraint with fixed dummy atoms. Side chains of residues that were taken into account, except for G-316 and A-317, were cut off from the CYP1A2 backbone, which was followed by replacing the flanking amides by hydrogens. The amide between the consecutive residues G-316 and A-317 was retained. Locations of Cα with attached three hydrogens and Cβ of included polar residues T-321, D-313, D-320, and T-498 as specified in Figure 3 were kept fixed. Polar residues T-124 and K-500 were shortened to β and δ carbons, respectively. Further, to maintain the particular environment of the catalytic center in CYP1A2, Cartesian coordinates of the portions of the side chains of lipophilic residues L-382, I-386 and L-497 starting with Cγ that are exposed to the catalytic center, as well as non-hydrogen atoms of the critical residue T-124[79] starting with Cβ were fixed at their X-ray positions. The rest of these residues down to Cα were removed. Atomic coordinates of the backbone fragment between G-316 and A-317 were fixed as well. It was noticed that in the minimum-energy structures of porphyrin-based molecular systems under investigation, Fe ion is located nearly in the center of the porphyrin ring, in line with previous studies.[67] Accordingly, to speed up geometry optimizations, Fe ion was maintained coplanar with chelating nitrogens of the porphyrin ring. The rest of the geometric variables of the complexes studied were optimized.

Two models have been utilized: large (L) and small (S) (Figure 3L and 3S, respectively). In model L, polar residues of both proton delivery systems (shown in red in PDS-1 and PDS-2), adjacent nonpolar residues (shown in green), as well as six water molecules (shown as red circles in

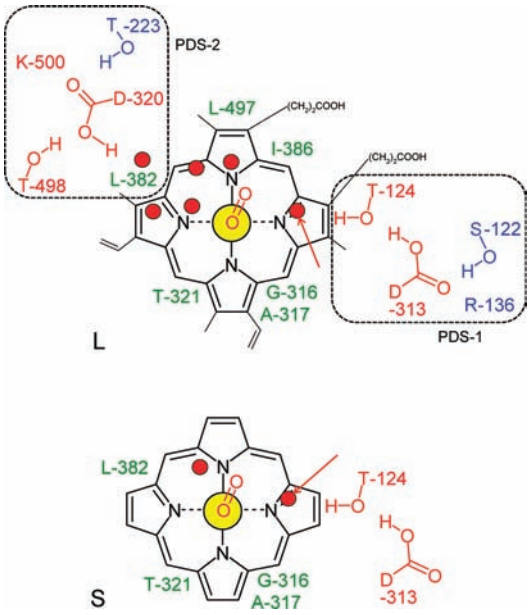

Figure 3. Models of the catalytic center of human CYP1A2 utilized for DFT-only calculations. Models L and S contained methyl-thiolate-ligated iron(III)−peroxo porphyrin complexes of CYP1A2. Thin bonds illustrate the CYP1A2 heme side chains, which were ignored in this study. Iron ion is illustrated as a yellow circle. Model L included six water molecules (shown as red circles), side chains of five polar residues (shown in red) from both proton delivery systems (framed and designated as PDS-1 and PDS-2), and side chains of six nonpolar boundary residues G-316, A-317, T-321, L-382, I-386, and L-497 (shown in green) as they appear in the X-ray crystallographic structure of human CYP1A2. Model S included two water molecules, side chains of two residues of PDS-1, and side chains of four boundary residues G-316, A-317, T-321, and L-382. The water molecule that is replaced by NH_2 of bound aromatic amine is shown by the red arrow in each model.

Figure 3L) that were necessary to fill the bottom of the catalytic cavity and thereby connect both PDSs to the catalytic center by proton transfer wires were included. A total of 11 residues adjacent to the catalytic center were thus incorporated into this model, with five of them being polar and six nonpolar. Polar residues represented the essential parts of PDSs. Nonpolar boundary residues were included to form the particular confinement for water molecules and substrates, inherent in the X-ray structure of human CYP1A2. To restrict conformational motion of the side chain of T-321 by the observed conformation, the backbone amide adjacent to A-317 that is H-bonded to OH of T-321 in the X-ray structure was included. This model was used to detect general changes in proton transfer wires preceding the first protonation from D-320-based PDS-2.

In model S (Figure 3S), which was used as a main computational tool to study energetics of catalytic reactions, PDS-2 was completely omitted together with the boundary residues I-386 and L-497, as the specific orientations of proton transfer wires along the reaction profiles were of the secondary importance for this study, and the main focus was made on binding modes and reactions of aromatic amines with the catalytic site of the enzyme. The side chain of T-321 was shortened, such that only the γ-CH_3 group, which is exposed to the catalytic center, was kept in this model as it is in the X-ray structure; accordingly, the A-317 flanking backbone amide was also removed and replaced by H. Binding modes of aromatic amines in the CYP1A2 cavity utilized were in line with predictions.[79] The water molecule replaced by an NH_2 group of bound aromatic amines is indicated by red arrows in both models. Only one water molecule from PDS-2 was retained in model S to eliminate an unfair stabilization of the anionic state of NH_2 group of aromatic amines

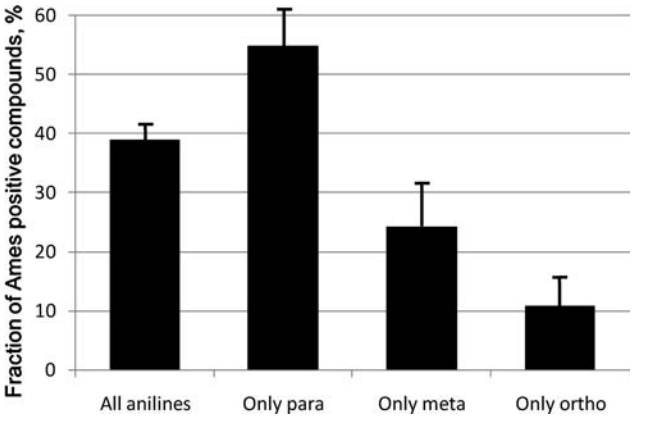

Figure 4. Fractions of mutagenic substituted anilines with primary amino groups in AstraZeneca in-house Ames mutagenicity database. The left column corresponds to all possible substitution patterns, and the rest of the histograms refer to the monosubstituted anilines of the indicated types. The error bars signify standard errors of the means.

with respect to the anionic oxygen of the ferric peroxo intermediate. No other residues of CYP1A2 were included in calculations, because they did not appear to be important for reaction profiles of aromatic amines of the considered classes (e.g., shown in blue in Figure 3L) or made the binding site too rigid for the DFT-only approach (e.g., F-226). DFT calculations were performed using the program Jaguar (version 9.2.109; Schrödinger Inc.). MP2 calculations were carried out using the program Gaussian 09.[80]

Tests for Bacterial Mutagenicity. Bacterial mutagenicity or "Ames" tests were performed by standard methods[81,82] with *Salmonella typhimurium* strains TA98 and TA100 using the plate incorporation method in the presence and absence of S9 from the livers of rats that treated with Aroclor 1254. All compounds were dissolved in dimethylsulfoxide (DMSO) and used within 2 h of preparation. Criteria for a positive result were 2-fold or 1.5-fold increases over the concurrent control for TA98 and TA100, respectively. The lower increase for TA100 was used because the solvent control value, mean 120−125, is greater than that for TA98, mean 30−35.

RESULTS AND DISCUSSION

It has been established that aniline itself is nonmutagenic.[83,84] Mutagenicity of substituted $ArNH_2$ is determined by the substitution pattern. To understand the physical origin of pro-mutagenic or protective effects of substituents, we start with actual experimental data. Fractions of Ames positive anilines in standard TA98/TA100 tester strains with primary amino groups in our AstraZeneca in-house Ames database are presented in Figure 4. These data represent all compounds that possess aniline or monosubstituted aniline as a substructure. As of today, we have a total of 346 substituted anilines of any substitution pattern, including 63 para, 33 meta, and 37 ortho monosubstituted compounds. These data suggest that the para position in anilines is the major place for pro-mutagenic substituents, whereas meta and ortho positions offer a better possibility to maintain substituted anilines nonmutagenic. These considerations are in agreement with a noticed narrow and elongated shape of the substrate binding cavity of CYP1A2 directed toward the catalytic center,[79] which is more suitable to accommodate large substituents of anilines placed in para position, rather than in meta or ortho. Available experimental data on mutagenicity of 2-aminopyridines do not allow us to draw reliable conclusions concerning the

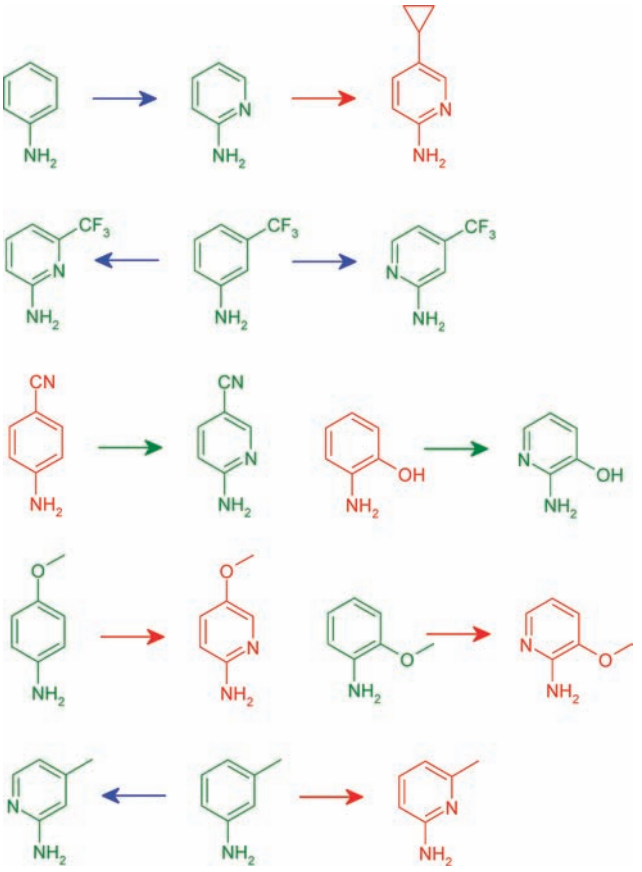

Figure 5. Examples of neutral, pro-mutagenic, and deactivating effects of 2-pyridine nitrogen in aromatic amines. Ames positive compounds are shown in red, while Ames negative compounds are in green. Neutral, pro-mutagenic, and deactivating structural alterations are illustrated by blue, red, and green arrows, respectively.

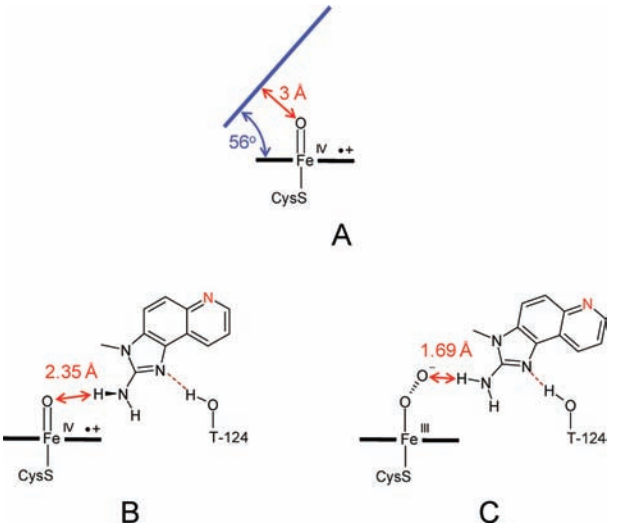

Figure 6. Intrinsic geometric features of the CYP1A2 substrate binding site for aromatic amines. (A) Mutual orientation of the planar substrate binding site (shown in blue) and Compound I derived from the X-ray structure of human CYP1A2.[79] (B and C) Results of DFT geometry-optimized calculations of simplified models of two catalytic forms of the CYP1A2 catalytic site with bound carcinogenic heteroaromatic amine 2-amino-3-methylimidazolo[4,5-*f*]quinoline (IQ): (B) neutral oxo-ferryl porphyrin π-cation radicaloid intermediate (Compound I); and (C) dianionic ferric peroxo intermediate. In these calculations, Model S of CYP1A2 (Figure 3S) was further simplified by removing all CYP1A2 residues except for T-124, and the location of the aromatic system of IQ was restricted by geometric constraints to be coplanar with α-naphthoflavone, a cocrystallized ligand in the X-ray structure of CYP1A2. Within the CYP1A2 fold, the active oxygen in Compound I (in B) is too far for H abstraction from NH_2 group of bound IQ, whereas the distant oxygen in the ferric peroxo intermediate (in C) can approach NH_2 group for strong H-bonding prior to proton abstraction. The pyridine-like N-atom, which is located in the resonance position in the third ring of IQ and increases mutagenic potency by 4 orders of magnitude,[33] is shown in red. This atom stabilizes the anionic form of IQ, thereby facilitating the proton abstraction.

overall effects of substitution patterns in this class. Nevertheless, it is clear that the pyridine-like N-atom significantly reduces the overall mutagenicity of 2-aminopyridines with respect to the overall level of anilines, from 39% ± 3% to 20% ± 4% (standard errors of the fractions of Ames positive compounds in our database are indicated). This is consistent with the pro-mutagenic nitrenium stabilization concept[50,58−60] as placing the electron-withdrawing N in resonance positions of aniline derivatives is known to destabilize nitrenium ions.[31,50,60] However, in many cases it is the pyridine-like N that makes 2-aminopyridines and similar polycyclic $ArNH_2$ mutagenic.[33,61] Figure 5 gives examples of neutral, inactivating, and activating effects of the aromatic nitrogen of 2-aminopyridines. Monosubstitution of nonmutagenic 2-aminiopyridine in any position can be pro-mutagenic. Generally speaking, the pyridine-like N of 2-aminopyridines dramatically changes the structure−mutagenicity relationship of $ArNH_2$ as illustrated in Figure 5. Para electron-withdrawing groups, which are pro-mutagenic in anilines, no longer activate 2-aminopyridines, whereas para π-electron donating groups do. Effects of ortho substitution in 2-aminopyridines are more pro-mutagenic than in anilines. To proceed with rational design of mutagenicity free $ArNH_2$, understanding the origin of the fundamental differences in structure−mutagenicity relationships between anilines and 2-aminopyridines is essential. In this Article, we focus on para substituted compounds of these two classes.

The catalytic cycle of cytochrome P450 enzymes has been studied for decades.[26,28,67,73,85,86] It is usually assumed that among several reactive intermediates that constitute the catalytic cycle, the oxenoid intermediate, the so-called Compound I (Figure 6A), is the most important form that oxidizes many, if not all substrates.[67] Existence of the second oxidant in P450 enzymes, apart from Compound I, has recently been suggested in several publications based on studies of the actual products of oxidation.[87−90] The second oxidant of P450 enzymes appears to be a ferric−hydroperoxide intermediate, Compound 0, which inserts hydroxyl cation, OH^+.

The mechanism of *N*-hydroxylation of the entire class of $ArNH_2$, which primarily occurs in CYP1A2 and, to a lesser extent, in CYP1A1, remains unknown.[3,39] Structures of two out of three members of human CYP1 family of P450 enzymes, CYP1A2 and CYP1B1, have been resolved by X-ray crystallographic analysis.[79,91] These structures reveal a new fold, in which binding sites for planar aromatic substrates are unusually separated from the catalytic center, which suggests that the oxenoid Compound I does not play the central role in oxidative reactions of planar substrates like polycyclic aromatic hydrocarbons, aflatoxins, and $ArNH_2$.[79] Indeed, assuming the Fe=O bond length in Compound I to be 1.65 Å, as

previously predicted,[67] the plane of aromatic substrate is separated from the oxenoid atom of Compound I roughly by 3 Å (Figure 6A). This is too far for efficient aromatic hydroxylation, "H abstraction−O rebound" or "direct O insertion", the major mechanisms that have been postulated for Compound I.[67,92−95] Moreover, if the binding modes of heteroaromatic amines are restricted by H-bonding of the pyridine-like N in α-position to residue T-124 as previously proposed,[79] their NH_2 groups are further separated from the reactive oxygen of Compound I. Optimized B3LYP/CSDZ* calculations that retained the mutual orientations of the porphyrin ring, the substrate binding site, and residue T-124 inherent in the CYP1A2 fold intact showed that the proximal oxygen of the catalytic center is located too far from NH_2 of carcinogenic heteroaromatic amine 2-amino-3-methylimidazolo-[4,5-*f*]quinoline (IQ) for efficient H abstraction (Figure 6B). On the other hand, the distal oxygen, for example, in the ferric peroxo intermediate, can be situated close enough to bound IQ to form a strong H-bond to NH_2 (Figure 6C). In addition, if *N*-hydroxylation of $ArNH_2$ proceeded through the "H abstraction−O rebound" mechanism, similar to *C*-hydroxylation of saturated hydrocarbons,[67,68] the CYP1 enzymes would be a factory of stable phenoxyl radicals, which are known to induce lipid peroxidation and oxidative stress.[96] Indeed, the H abstraction step is even easier in phenols than in anilines,[97] but the second, O rebound, step, which is supposed to recombine aminyl and OH radicals, would be impossible for phenoxyl radicals because the O−O bond being adjacent to an aromatic system is unstable. One could speculate that the reason for the special fold in CYP1 family of enzymes, which is designed to oxidize aromatic compounds, is to prevent uncontrolled H abstraction from phenolic substrates by Compound I.

Because bacterial mutagenic potency in many classes of $ArNH_2$ is linked to electron affinity that increases by addition of electron-withdrawing groups,[13,29,39,61] one could hypothesize involvement of the rate-determining formation of anionic forms in the activation mechanism. There is only one intermediate in the catalytic cycle that is able to abstract protons from NH_2 groups of the entire class of aromatic amines. It is the dianionic ferric peroxo intermediate, $(CYP1A2)Fe^{III}-OO^-$, because the proton affinity of this oxidant (422 kcal/mol[67]) far exceeds typical heterolytic dissociation energy of NH bonds in $ArNH_2$ (350−390 kcal/mol) as calculated at the B3LYP/6-31G* level of theory. This particular oxidant has been previously shown to participate in P450-catalyzed nucleophilic reactions, such as oxidative decarbonylation of aldehydes and in the biosynthesis of estrone.[73] If this oxidant is also involved in metabolic activation of $ArNH_2$, chemical events that follow the initial proton abstraction and formation of ferric-hydroperoxide-based Compound 0, $(CYP1A2)Fe^{III}-OOH$, would certainly be dependent on the stability of the anionic forms of $ArNH_2$ and concomitantly on the electron affinity of parent $ArNH_2$. Besides, this would be in line with previously hypothesized involvement of OH^+ in catalytic mechanisms of P450 enzymes[89] and consistent with general propensity of peroxide moieties for heterolytic cleavage in the framework of S_N2 mechanism.[98] Reaction profiles of protonation of ferric peroxo oxidant are known to be sensitive to the environment, such as the number of included water molecules and adjacent residues;[67] however, the absolute values of energetics do not matter for this study, which is focused on relative effects of different substrates.

Figure 3 illustrates close proximity of the catalytic machinery of human CYP1A2 in the ferric peroxo state. There are two proton delivery systems (PDS-1 and PDS-2) in the enzyme that fit the general description of such systems in P450 enzymes.[67,99] Protonation of a basic residue that is always present in such systems triggers spontaneous proton transfer from the protonated acidic residue to the bound catalytic oxygen.[99] In P450 enzymes, there is always a gap between the residue that acts as a source of proton and the catalytic oxygen,[100] and proton transfer wires have to incorporate the OH group of Ser or Thr and/or polarized H-bonded water chains.[67,101] Figure 1S-A gives the DFT-optimized structure of model L in the ferric peroxo state with six water molecules, which are necessary to fill the available confinement at the bottom of the catalytic site and connect both PDSs to the catalytic oxygen. As is seen, both PDSs in the ferric peroxo intermediate are connected to the same distal negatively charged catalytic oxygen through proton transfer wires, such that four water molecules are directly H-bonded to the distal oxygen. Results suggest that the D-313 centered PDS-1 is designed to transfer proton through OH group of T-124 using a single water molecule. Because D-320, the central residue of PDS-2 of CYP1A2, is located further away from the catalytic machinery, the resultant proton transfer wire contains five water molecules and likely splits into three wires (Figure 1S-A). The basic assumption that we have to make is that protonation of the ferric peroxo intermediate in CYP1A2 is generally the rate-limiting step in metabolism of $ArNH_2$, which allows protonation of the distal oxygen to occur from the bound aromatic amines, rather than from PDS of the enzyme. Although the rate-limiting step in *N*-hydroxylation of $ArNH_2$ is not yet identified, this assumption is consistent with kinetics measurements in other P450 enzymes.[102] Figure 1S-B gives the DFT-optimized structure of model L, in which the single water molecule that mediates proton transfer from PDS-1 is replaced by NH_2 of mutagenic compound, 5-methoxypyridin-2-amine. As is seen, NH_2 of bound $ArNH_2$ binds to the same place as the replaced water molecule, but is unable to mediate proton transfer from the D-313 based PDS-1. On the other hand, this particular binding mode maintains the proton transfer wire from D-320-based PDS-2 intact, which is consistent with side directed mutagenesis studies that demonstrated that residue D-320 is important for metabolism of aromatic amines.[28]

Structures of focused $ArNH_2$ considered in this study are shown in Figure 7. Figure 8A shows the B3LYP/CSDZ* energy of water replacement by substituted anilines and 2-aminopyridines in model S of the ferric peroxo intermediate of human CYP1A2 before (eq 1) and after (eq 2) proton abstraction as a function of relative stabilities of the anionic forms of $ArNH_2$. Because the B3LYP functional does not take dispersion interactions into account,[103] the energy balance given by eq 1 only indicates relative H-bonding capacity of aromatic amines versus water molecule. As is seen, the single water molecule is much more efficient in H-bonding to the enzymatic site of CYP1A2 than NH_2 of aniline and all para-substituted compounds based on the anilinic scaffold. Naturally, other attractive components of binding energy, that is, van der Waals, $\pi-\pi$, and hydrophobic interactions, which play major parts in bringing mutagenic aromatic amines to the enzymatic site, make the overall free energy balance negative. However, the fact that nonmutagenic aniline turns out to be least effective in replacing the water molecule in the considered classes is suggestive of a possible reason for its inactivity. Both electron-withdrawing groups like F, CF_3, and CN, and π-electron donating group, OCH_3, in para position of aniline facilitate water replacement and, simultaneously, increase mutagenicity. Both of these types of functions as well as the additional benzene ring increase the dipole moment

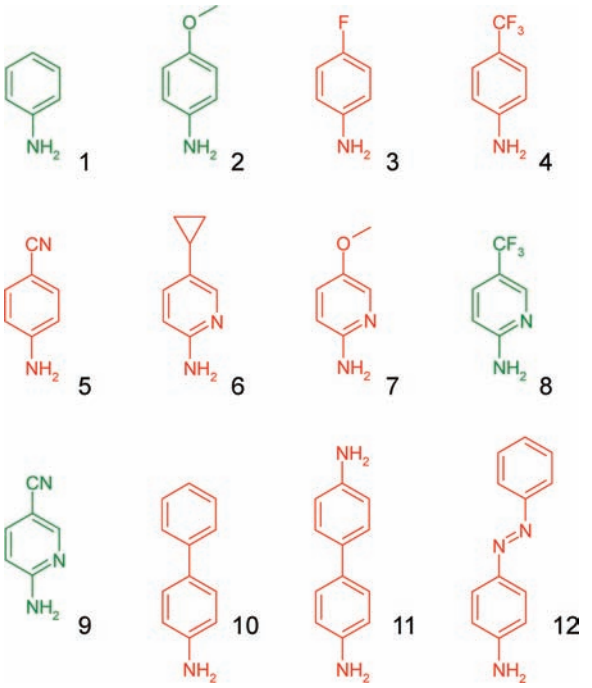

Figure 7. Structures of focused aromatic amines. Ames positive and Ames negative aromatic amines in TA98/TA100 strains are shown in red and green, respectively.

of aniline, such that the positive end of the dipole is situated closer to the dianionic enzymatic center. According to the B3LYP/6-31G* results, dipole moments of aniline **1**, 4-fluoroaniline **3**, 4-methoxyaniline **2**, and 4-aminobiphenyl **10** are 1.71, 2.83, 1.80, and 2.13 D, respectively. The role of dipole moment of $ArNH_2$ in increasing mutagenic potency has been previously noted.[39,61] In addition, both electron-withdrawing functions and extension of the aromatic system amplify acidity of NH_2 group, thereby further increasing H-bonding capacity of $ArNH_2$ in the enzymatic site as H-bond donors (Figure 6C). It should be noted that compounds **2** and **3** that flank inactive aniline in both axes in Figure 8A are very weak mutagens.[104,105] Mutagenicity of **2** could be unequivocally established only in bacterial strains containing elevated activity of *N*-acetyltransferase.[106] The second aromatic ring further facilitates replacement of the water molecule from the binding site with respect to data presented in Figure 8A because more mutagenic bicyclic $ArNH_2$ form more attractive interactions with the enzymatic cavity than monocyclic compounds, specifically with aromatic residues F125, F226, F256, and F260 of CYP1A2, which are beyond the model systems utilized. The primary factor (F1) of mutagenicity of $ArNH_2$ is stability of the productive binding mode in CYP1A2 (Figure 8), which increases residence time and thereby assists in proton abstraction.

$$(CYP1A2)Fe^{III}{-}OO^{-}:H_2O + ArNH_2 \rightleftharpoons (CYP1A2)Fe^{III}{-}OO^{-}:ArNH_2 + H_2O \quad (1)$$

$$(CYP1A2)Fe^{III}{-}OO^{-}:H_2O + ArNH_2 \rightleftharpoons (CYP1A2)Fe^{III}{-}OOH:ArNH^{-} + H_2O \quad (2)$$

As expected, 2-aminopyridines form more stable complexes with the ferric peroxo intermediate of CYP1A2 than do anilines

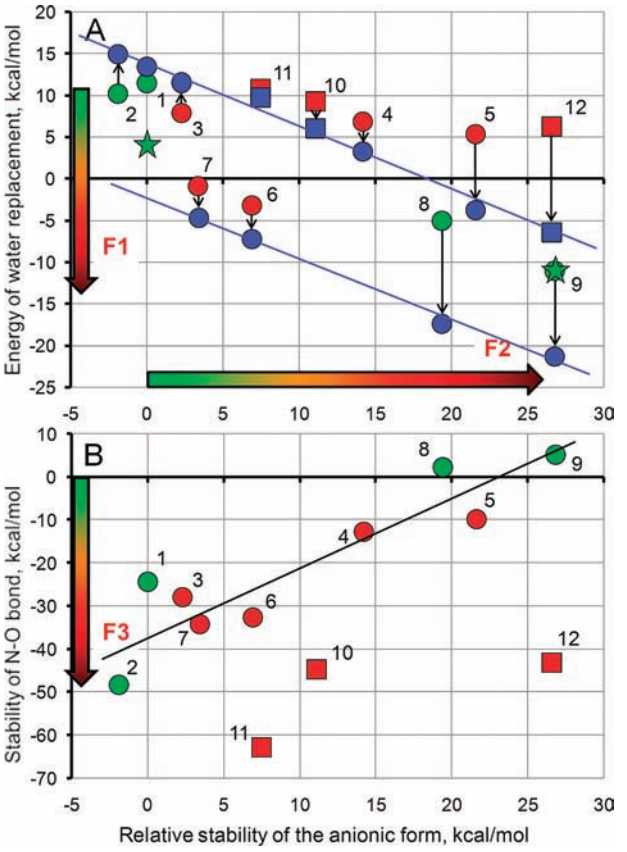

Figure 8. Results of optimized DFT calculations. (A) Energy of replacement of the H-bonded water molecule in the enzymatic site of CYP1A2 by NH_2 of aromatic amines according to eq 1 in Model S versus relative stability of their anionic forms, $ArNH^{-}$. Stability of the anionic form of aniline **1** was set to 0. Energy of water replacement plus subsequent proton abstraction from NH_2 of aromatic amines according to eq 2 is illustrated in blue. Black vertical arrows signify energy of the proton abstraction (endothermic − up, exothermic − down). Energies of the anionic states of bound anilinic and 2-aminopyridinic subclasses fit to the straight lines shown in blue. Water replacement energies for **1**and **9** obtained at the M06-2X/6-31+G* level are shown by green stars. (B) Stability of N−O bonds of hydroxylamines for proton-assisted heterolytic dissociation according to eq 3 versus relative stability of the anionic forms. Ames positive compounds are shown in red, while Ames negative are in green. Monocyclic compounds are shown as circles, while bicyclic are shown as squares. Numbers correspond to the numeration of focused aromatic amines in Figure 7. The black straight line fits to data obtained for monocyclic aromatic amines. Thick arrows show major factors that make aromatic amines mutagenic: F1, stability of the productive binding mode of aromatic amines in CYP1A2 substrate site; F2, ease of proton abstraction from aromatic amines; and F3, instability of N−O bond of hydroxylamine for hydrolytic dissociation under acidic conditions.

because of the additional H-bonding of pyridine-type nitrogen to T-124.[79] This H-bonding increases the stabilization energy of the complex by about 12 kcal/mol and makes binding of 2-aminopyridines binding of the ferric peroxo intermediate significantly more favorable than binding of the water molecule (Figure 8A). The corresponding increase of residence time with respect to anilines is likely to explain pro-mutagenic effects of this N (Figure 5). It should be noted that this activation is especially impressive because it overrides two previously described deactivating factors caused by this atom, decreasing of compound lipophilicity[10,107]

and destabilization of nitrenium ions.[31,50] Energy of water molecule replacement, which was calculated using eq 1 and model L, gave similar results. Thus, binding energies of compounds **1** and **7** in model S were obtained to be 11.5 and −0.8 kcal/mol, respectively, whereas in model L they were equal to 14.4 and −0.6 kcal/mol, respectively.

As is seen in Figure 8A, the stability of anionic forms in both considered classes of $ArNH_2$ significantly increases by strong para electron-withdrawing groups, like CF_3 or CN, and the second aromatic ring, but their electron-withdrawing power does not produce the corresponding effect on the stability of the complex with ferric peroxo intermediate. On the contrary, after proton abstraction from $ArNH_2$, the electron-withdrawing propensity of para substituents drastically increases the stability of the complexes of the resultant anionic species with ferric−hydroperoxide intermediate. Complex stabilization increases as a linear function of intrinsic resonance stabilization of the anionic form of $ArNH_2$. As a result, the energy gain upon proton abstraction from $ArNH_2$ dramatically increases by electron-withdrawing groups and the second aromatic ring in para position; being somewhat endothermic with OCH_3, H, and F, it becomes strongly exothermic with CF_3 or CN, and in 4-aminoazobenzene **12**. Stabilization of bound anionic forms of anilines in the enzymatic site of CYP1A2 is closely linked to activation of their mutagenicity by electron-withdrawing groups, with the presence of the pyridine-type nitrogen in resonance position in 2-aminopyridines being a part of this very trend. This makes the ease of proton abstraction the second factor (F2) of mutagenicity of $ArNH_2$.

Surprisingly, the effect of strong electron-withdrawing groups CF_3 or CN on mutagenicity of 2-aminopyridines is opposite; that is, instead of boosting mutagenicity of **8** and **9** like in the anilinic analogues **4** and **5**, they remove it. On the other hand, the π-electron-donating group OCH_3 keeps **7** mutagenic, unlike in the anilinic class. In the 2-aminopyridinic class, the anionic forms are already stabilized by the pyridine-type nitrogen. This suggests that apart from stabilization of complexes of neutral and anionic forms of $ArNH_2$ within the enzymatic site (Figure 8A), there should be another factor working in the opposite direction, which plays an important role only when anionic forms in monocyclic $ArNH_2$ are too stable.

Figure 8B gives the stability of N−O bond in hydroxylamines for acid-catalyzed heterolytic dissociation calculated as the energy of reaction 3 versus relative stability of the anionic forms of parent $ArNH_2$. Involvement of transient protonation in heterolytic dissociation of hydroxylamines of anilinic $ArNH_2$ in water has been demonstrated.[6,31,108]

$$ArNHOH + H_3O^+ \rightleftharpoons ArNH^+ + 2H_2O \quad (3)$$

$$ArNHOC(O)CH_3 + H_3O^+ \rightleftharpoons ArNH^+ + H_2O + HOC(O)CH_3 \quad (4)$$

$$ArNHOSO_3H + H_3O^+ \rightleftharpoons ArNH^+ + H_2O + H_2SO_4 \quad (5)$$

The N−O bond in hydroxylamines of monocyclic $ArNH_2$ becomes more stable almost linearly with stabilization of the anionic forms. There is no surprise in this trend: substituents that stabilize the anion destabilize the nitrenium ion. As is seen, dramatic stabilization of the anionic form of monocyclic $ArNH_2$ **8** and **9** by electron-withdrawing functions in two resonance positions makes heterolytic dissociation of hydroxylamines in reaction 3 endothermic, such that the ultimate DNA-reactive electrophilic forms of $ArNH_2$ are never formed to attack DNA bases. However, the second aromatic ring stabilizes both anionic and cationic forms of $ArNH_2$, which facilitates metabolic activation of polycyclic conjugated aromatic amines all the way to nitrenium ions (Figure 1), consistent with previous studies that demonstrated that the extent of the aromatic system is one of the most important descriptors in mutagenicity of $ArNH_2$.[39] This makes the stability of N−O bond in hydroxylamines the third factor (F3) of mutagenicity of aromatic amines. This factor is far from being anything new,[50,56−60] but confusing results that have been obtained by previous attempts to directly correlate mutagenic potency to stability of nitrenium ions in wide sets of $ArNH_2$[33,60] have been likely caused by underestimation of the importance of the anionic forms that respond to inductive and mesomeric substituents in resonance positions in the opposite way. Bioconjugation of hydroxylamines by Phase II enzymes, such as arylamine *N*-acetyltransferase (NAT) and sulfotransferase (SULT), is thought to catalyze hydrolytic dissociation of the N−O bonds to DNA-reactive nitrenium ions.[6] Thus, it has been found that mutagenic potencies of $ArNH_2$ can be increased by up to 250-fold in bacterial strains that have been engineered to express NAT or SULT proteins.[6] Consistent with these observations, calculations of reaction energies of proton-assisted heterolytic dissociation of the resulting *O*-acetylates (ArNHOAc) and sulfates ($ArNHOSO_3H$) of different hydroxylamines according to eqs 4 and 5 at the B3LYP/6-31G* level of theory showed that acetylation and sulfation consistently weaken the N−O bonds by 4.1 ± 0.3 and 4.8 ± 0.5 kcal/mol, respectively.

Thus, the results suggest that a balance of three critical factors contributes to $ArNH_2$ mutagenicity: binding affinity of their productive conformations in the catalytic cavity of CYP1A2 prior to proton abstraction (F1), the ease of proton abstraction (F2), and the susceptibility of the N−O bonds in the resultant hydroxylamines to proton-assisted heterolytic dissociation (F3). The contribution of individual factors to the overall mutagenic potency of an $ArNH_2$ varies and decreases in the sequence F1 > F2 > F3. The factors do not act simultaneously, but strictly sequentially in that particular order according to the sequence of chemical events in the proposed metabolic activation mechanism, and if one of these factors is disrupted for a particular $ArNH_2$, the following factors do not matter. For example, the hydroxylamine from aniline is vulnerable enough to form reactive nitrenium ion (Figure 8B), but it seems unable to replace the water molecule from the catalytic site to form that hydroxylamine, which makes aniline mutagenicity free. Both binding affinity in CYP1A2 and the ease of proton abstraction are disrupted for **2**, and the fact that it forms particularly stable nitrenium ion does not make it unequivocally mutagenic.[106] The role of stability of nitrenium ions (F3) in mutagenicity of $ArNH_2$ of different classes has recently been re-evaluated in a large data set.[57] The results indicated that only a minor discrimination between mutagenic and nonmutagenic compounds is possible when using this factor alone.

Chemical events in the metabolic activation pathway of the considered classes of $ArNH_2$ in CYP1A2 that follow proton abstraction by the ferric peroxo intermediate are all exothermic and inevitably lead to DNA-reactive hydroxylamines for all $ArNH_2$. Thus, they do not affect structure−mutagenicity relationships of $ArNH_2$ beyond liability of N−O bonds of hydroxylamines for heterolytic dissociation. However, according to our

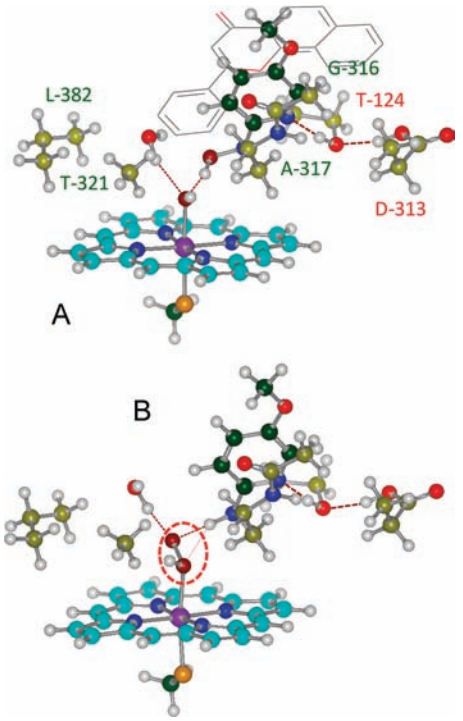

Figure 9. DFT-optimized structures of model S of products A and B of the first protonation of the ferric−hydroperoxide intermediate of CYP1A2 with bound anionic form of aromatic amine **7**. Structures of the products are given in Figure 10. (A) Hydroxylamine with Compound II; (B) the hydroperoxy radical releasing product. The obtained binding modes of the metabolites of the ligand are coplanar with the position of α-naphthoflavone in the X-ray structure of CYP1A2,[79] which is illustrated in (A) with thin lines. Residue numbers of CYP1A2 are designated in (A) only. Hydroperoxy radical is encircled in (B). Carbon atoms of porphyrin ring are shown in cyan, Fe cation in magenta, hydrogens in white, carbons of adjacent side chains in light green, other carbons in dark green, sulfur in orange, oxygens in red, nitrogens in blue, and oxygens derived from the catalytic dioxygen in dark red. Hydrogen bonds are shown in dark red.

calculations, other species can also be formed apart from hydroxylamines. Results of DFT geometry optimizations within model L suggest that protonation of basic residue K-500 of PDS-2 that is H-bonded to protonated D-320 in CYP1A2 triggers barrier-free proton transfer along the proton transfer wires toward the catalytic center (Figures 3 and 1S). Further, studies of model L with bound mutagenic compound **7** indicated that the network of H-bonded water molecules is rewired upon proton abstraction. Before proton abstraction, all proton transfer wires connected protonated D-320 with the negatively charged distal oxygen of the ferric peroxo intermediate (Figure 1S-B). Because the negative charge of the distal oxygen of the ferric peroxo intermediate is removed after proton abstraction and relocated to the anionic N of $ArNH^-$, proton transfer wires are rewired to incorporate both the proximal oxygen of the oxidant and the anionic N into the H-bonded network (Figure 1S-C). Therefore, possible targets for the proton transfer, which is supposed to follow the proton abstraction event, have to include both oxygens of the ferric−hydroperoxide moiety and the anionic N of bound $ArNH^-$. It has been established that targets of the proton transfer through polarized H-bonded water chains are determined both by thermodynamics of the products and by kinetics of the proton transfer routes.[101] Because dynamics of proton transfer wires could not be possibly taken into consideration at the present time, we had to consider protonation of all three target atoms and rely on the thermodynamic stability of the products.

Figure 9 illustrates geometry-optimized 3D structures of products A and B of the first protonation event within model S with mutagenic compound **7**, and Figure 2S gives structures C and D. Figure 10 shows their structures, and Figure 11 gives their energy levels with respect to hydroxylamines for eight monocyclic $ArNH_2$. In all four products (Figures 9 and 2S), the DFT-optimized planes of 2-aminopyridine rings coincide with the position and orientation of the plane of α-naphthoflavone with respect to the position of heme in the X-ray structure of CYP1A2.[79] This suggests that the unusual situation of the substrate binding site in CYP1A2, which makes an angle of 56° with the plane of the porphyrin ring (Figure 6A), is made optimal for hydroxylamines, the main metabolites of aromatic amines, which likely facilitates the intended chemical transformations.

Protonation of the proximal oxygen of Compound 0 dramatically weakens both O−O and O−H bonds of the hydroperoxide moiety for heterolytic dissociation and results in mutagenic products, hydroxylamines (A) and hydroperoxy radical (B) (Figure 10). Cleavage of the O−O bond leads to hydroxylamine, in line with the proton-catalyzed S_N2 mechanism common in peroxide chemistry[98] with a small activation barrier. According to MP2/6-311+G*//B3LYP/6-31G* calculations, the heterolytic O−H bond dissociation energy of Compound 0 is 428 kcal/mol, which exceeds the heterolytic N−H bond dissociation energy of aniline by 55 kcal/mol. This difference represents the thermodynamic driving force for the proton abstraction event from aniline to the ferric peroxo intermediate. After the proximal protonation of Compound 0, the heterolytic dissociation energy of O−H bond decreases to 355 kcal/mol, which is below the dissociation energy of the N−H bond in aniline by 18 kcal/mol. This may represent the thermodynamic driving force for returning the abstracted proton back to the anionic form of $ArNH_2$, especially if the N−H bond is strengthened by π-electron donating groups. Heterolytic cleavage of the O−H bond leads to the formation of bound hydroperoxy radical. It should be noted that this route retains intact $ArNH_2$ bound to the CYP1A2 substrate binding site, which implies that this $ArNH_2$ acts as a catalyst of the transformation of O_2 to ·OOH. This could be the reason for oxidative stress caused by interactions of particular $ArNH_2$ with CYP1A2.[43] Protonation of both the distal oxygen of the hydroperoxide moiety and the anionic N of $ArNH^-$ finally results in regeneration of the parent $ArNH_2$ bound to Compound I and Compound 0 of the enzyme (structures C and D, respectively). In nearly all considered cases, the most stable product is hydroxylamine H-bonded to Compound II (structure A in Figure 10 and red circles in Figure 11). Stability of the second complex (B), which releases hydroperoxy radical (blue circles in Figure 11), is significantly above the hydroxylamine level for all considered $ArNH_2$ except for aniline **1** and 4-methoxyaniline **2**. Thus, π-electron-donating groups in para resonance position in the anilinic subclass increase proton affinity of the anionic forms, which facilitates regaining the lost proton from the protonated ferric-hydroperoxide intermediate, thereby releasing free radical, in line with experimental data.[43] Figure 12 illustrates the way the described routes of metabolic activation of $ArNH_2$ are incorporated in the catalytic cycle of CYP1A2. It should be noted that proximal protonation of Compound 0 as a critical step of the hypothesized second catalytic mechanism of P450 enzymes has been previously suggested.[87]

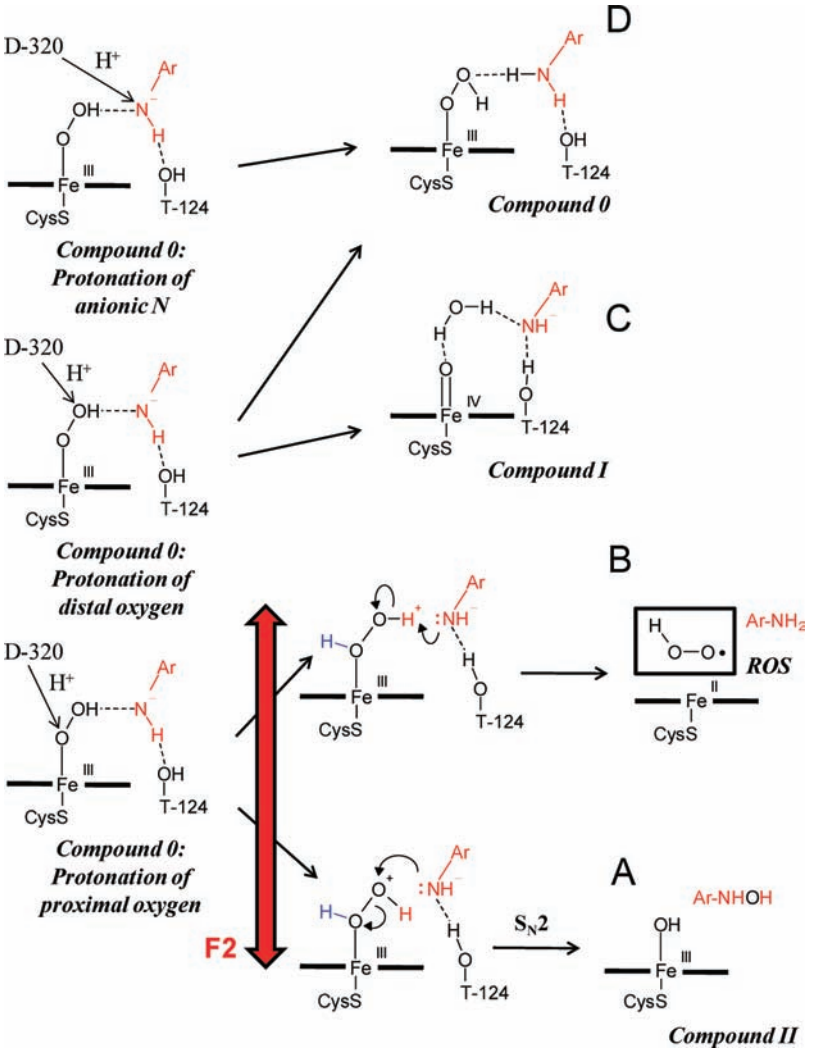

Figure 10. Reaction intermediates of metabolism of aromatic amines in CYP1A2 following the first protonation by the D-320 centered PDS-2. Three possible targets of protonation lead to four products H-bonded to the catalytic center (A−D). Relative fraction of mutagenic products, hydroxylamines and hydroperoxy radicals, is predicted to be determined by the factor F2, that is, by stability of the anionic form of aromatic amines. Two-sided arrow indicates that both stabilization and destabilization of the anionic form by itself is unable to remove mutagenicity of the metabolites of aromatic amines.

The main results obtained by B3LYP/6-31G* calculations and presented in Figures 8 and 11 were validated using higher levels of theory. Tables 1 and 2 represent validation of predicted properties of reaction intermediates of individual $ArNH_2$; Table 3 confirms that relative proton affinities of the anionic forms of the oxidant and $ArNH_2$ are well balanced along the metabolic activation pathway; Figures 8A and 11 include data obtained by geometry-optimized M06-2X/6-31+G* calculations. Table 1 presents heterolytic bond dissociation energies of N−H bonds in five selected $ArNH_2$ and energies of proton-assisted heterolytic cleavage of N−O bonds in their hydroxylamines according to eq 3 predicted by MP2/6-311++G(2df,2p) and MP2/6-311+G*//B3LYP/6-31G* calculations. The N−H bond dissociation energies of $ArNH_2$ obtained at these levels of theory are very similar, but the single-point MP2 calculations based on the B3LYP/6-31G* geometries exhibit rather high errors in energies of N−O cleavage with respect to the fully optimized higher MP2 level. Table 2 presents the corresponding values obtained by fully optimized DFT calculations. These data illustrate that the B3LYP/6-31G* level of theory consistently overestimates the heterolytic N−H bond energy by roughly 10 kcal/mol with respect to the MP2 calculations, whereas the addition of diffuse functions to the basis set within this or within the more sophisticated functional, M06-2X, resolves the inconsistency, in line with previous studies that showed the importance of diffuse functions for description of anions.[76] Nevertheless, relative stabilities of the anionic forms seem to be very similar at all employed levels of theory. The B3LYP/6-31G* level appears to be the best to describe the energy of N−O bond cleavage predicted by fully optimized MP2/6-311++G(2df,2p) calculations. Notably, eq 3, which these data are obtained from, does not include anionic species. Thus, results suggest that data presented in Figure 8B are consistent with results obtained at higher theoretical approximations.

Because the proposed mechanism is based on thermodynamics of proton abstraction events, it is critical to validate the predicted balance of proton affinities of the anionic forms of the oxidant and $ArNH_2$ along the metabolic activation pathway using higher levels of theory. Table 3 gives heterolytic bond dissociation energies obtained at different DFT and ab initio levels using the B3LYP/6-31G*-optimized geometries of the relevant states

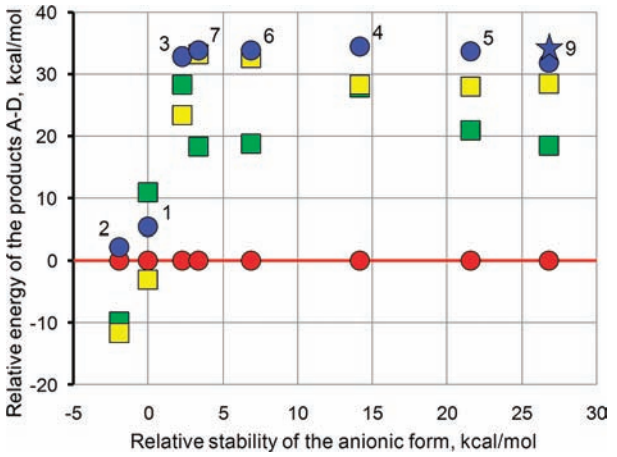

Figure 11. Relative energies of the products (A−D) of the first protonation of the ferric−hydroperoxide intermediate of Model S of CYP1A2 with bound anionic aromatic amines as a function of relative stability of the anionic forms: hydroxylamine (A), radical releasing complex (B), as well as Compound I (C)- and Compound 0 (D)-based complexes (structures are shown in Figure 10). Products that result from protonation of the proximal (A,B) and distal (C,D) oxygen atoms of the ferric−hydroperoxide intermediate are shown in circles and squares, respectively. Stability of the anionic form of aniline was set to 0. Energy of the product A was set to 0 for all molecules. Results obtained for products A, B, C, and D are shown in red, blue, green, and yellow, respectively. The hydroperoxy radical releasing states (B) are numbered according to Figure 7; the rest of the products of the same aromatic amine are shown on the same vertical line. Relative stability of the B form of **9** obtained at the M06-2X/6-31+G* level of theory is shown by the blue star.

of the oxidant. As is seen, the absolute values of the O−H bond dissociation energies of the oxidant are also overestimated by the B3LYP/6-31G* calculations, whereas the B3LYP/6-31+G* and M06-2X/6-31+G* approximations reproduce values predicted at the MP2/6-311+G* level. On the other hand, the relative O−H bond dissociation energies obtained at the MP2/6-311+G* level are reproduced by B3LYP/6-31G* calculations reasonably well.

Geometry optimization of porphyrin-based complexes with bound metabolites of $ArNH_2$ is much more difficult when using levels of theory higher than the B3LYP/CSDZ*. Energies of water replacement in the model S of ferric peroxo intermediate by **1** and **9** were calculated by eq 1 using energy optimizations at the M06-2X/6-31+G* level, because the standard B3LYP functional was suspected to underestimate attractive dispersion interactions of the complexes. Results are illustrated in Figure 8A. As expected, the complex with H-bonded aniline **1** appeared more stable at the M06-2X/6-31+G* level, with the energy balance of eq 1 still being endothermic (energy decreased from 11.5 to 3.7 kcal/mol), whereas very minor changes in energy were obtained for **9** (energy increased from −11.1 to −10.9). This suggests that dispersion interactions are important for stabilization energies of complexes of $ArNH_2$ of the anilinic class but not important for $ArNH_2$ of the 2-aminopyridinic class. Geometry optimizations of these test complexes at the M06-2X/6-31+G* level resulted in only minor changes with respect to the B3LYP/6-31G*-optimized structures. The aromatic rings of bound **1** and **9** are located somewhat closer to the juxtaposed G-316−A-317 fragment of CYP1A2 at the M06-2X/6-31+G* level because of attractive van der Waals interactions, which could not be taken into account at the B3LYP/6-31G* level. The relative stability of products A and B of **9** did not significantly change when using the energy-optimized M06-2X/6-31+G* level of theory (Figure 11). Thus, the B3LYP/6-31G* results are reasonably reliable. It should be noted that water replacement energies of all $ArNH_2$ of the anilinic class are likely more exothermic than they appear in Figure 8A, as expected and confirmed by more reliable energy-optimized calculations at the M06-2X/6-31+G* level of theory.

To sum, the mechanism of metabolic activation of $ArNH_2$ by CYP1A2 to hydroxylamines is likely to proceed through rate-determining proton abstraction with subsequent binding of $ArNH^-$ to OH^+ in a concerted S_N2 fashion. The proposed mechanism is consistent with the general importance of electron affinity in mutagenic potency of $ArNH_2$. Within this mechanism, we identified two factors that facilitate the metabolic pathway: the binding affinity of $ArNH_2$ in CYP1A2 in a productive binding mode and the ease of proton abstraction from $ArNH_2$. A subsequent variable, exothermicity of proton-assisted heterolytic dissociation of N−O bond, favors converting the resulting hydroxylamines to the DNA-reactive nitrenium ions.

This being the case, we have to find the reflections of the effects of these three factors in the observed structure−mutagenicity relationships in the entire class of $ArNH_2$ beyond the focused compounds. In the worst case, when all three promutagenic factors work flawlessly, the amount of produced nitrenium ions and, consequently, DNA adducts and DNA mutations will be maximal. This will likely make such $ArNH_2$ carcinogenic. A formal description of such hypothetical highly mutagenic compounds indeed leads us to carcinogenic quasi-planar polycyclic $ArNH_2$ like 4-aminobiphenyl, 2-aminofluorene, 2-aminonaphthalene, and two known classes of cooked-food carcinogenic polycyclic heteroaromatic amines, that is, aminocarbolines and amino-imidazoazaarenes.[13,33] The most mutagenic compounds of these classes fit to the CYP1A2 substrate cavity in the required binding mode particularly well because they are polycyclic and nearly planar. Besides, conjugated polycyclic aromatic amines have an intrinsic propensity of forming especially stable both anionic and cationic forms (Figure 8B). In addition, food-derived heteroaromatic amines possess the pyridine-type N in α-position with respect to the amino group, which stabilizes their productive binding mode by H-bonding to T-124, similar to 2-aminopyridines (Figure 1S-B). It should be emphasized that the electronegative pyridine-like N-atoms, which are present in all food-derived heteroaromatic amine mutagens and often increase their mutagenic potency by several orders of magnitude, do not stabilize the nitrenium ion[33] but stabilize the anionic form. The mutagenicity boosting effects of such nitrogens are especially impressive when they are located in distant resonance positions with respect to the NH_2 group, like in the third ring of IQ (Figure 6C) or in the second ring of 2-amino-1-methyl-6-phenylimidazolo[4,5-*b*]pyridine (PhIP).[13,33]

The cause of remarkable effects of the resonance locations of pyridine-like nitrogen and phenyl ring in polycyclic heteroaromatic amines has been investigated in detail in a comparative study of PhIP and its isomer 3-Me PhIP, where these functions are situated in nonresonance places.[13] It has been shown that the resonance location of these functions accelerates the *N*-hydroxylation of $ArNH_2$ in rat liver microsomes by 5 times, whereas the overall effect on mutagenic potency in the Ames assay is about 20 times higher. The remaining 20-fold difference is ascribed to the mutagenic potencies of hydroxylamines.[13] Lau et al. studied energetics of the *O*-acetylation of hydroxylamines of polycyclic

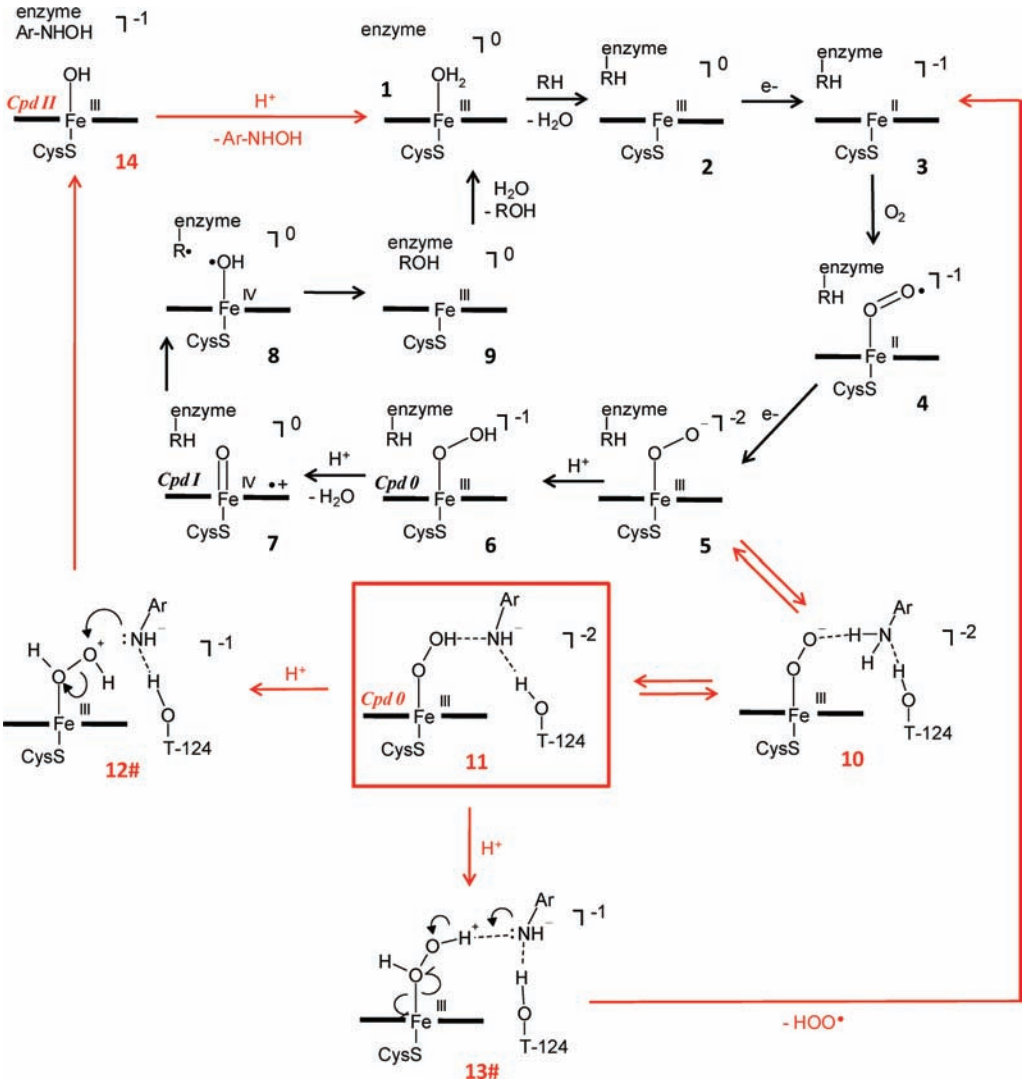

Figure 12. The suggested mechanisms of metabolic activation of aromatic amines in CYP1A2 (indicated by intermediates **10**−**14** connected by red arrows) incorporated into the standard catalytic cycle of P450 enzymes (intermediates **1**−**9**).[67] The total charge is shown at the top right corner of each intermediate. The intermediate **10** illustrates the productive binding mode of aromatic amine in the ferric peroxo intermediate prior to proton abstraction. The mutagenic potency determining step, which is facilitated by electron-withdrawing groups, is framed and designated **11**. The *N*-hydroxylation pathway is **5**−**10**−**11**−**12#**−**14**−**1**. The ROS generation pathway is **5**−**10**−**11**−**13#**−**3**.

heteroaromatic amines in human NAT by DFT calculations to shed light on the origin of this effect.[109] The authors demonstrated that *O*-acetylation of neutral hydroxylamines is hindered by a high activation barrier, whereas the reaction of their anionic forms would be facile. Therefore, it is tempting to assume that *O*-acetylation of hydroxylamines in NAT follows the transient deprotonation, just like in the proposed mechanism in CYP1A2. The typical cysteine protease-like catalytic triad inherent in human NAT, that is, C-68−H-107−D-122,[110] which is designed for deprotonation of thiol of C-68,[111,112] could also deprotonate hydroxylamines because heterolytic bond dissociation energies of S−H in cysteine and O−H in ArNHOH are similar (Figure 13), and because putative binding modes of hydroxylamines place the N−OH groups close to the catalytic triad.[109,110] Therefore, the assumption that the *O*-acetylation in NAT might undergo the rate-determining proton abstraction from hydroxylamines seems reasonable. Figure 13C presents relative anionic stabilities of $ArNH^-$ and $ArNHO^-$ of the focused compounds and two relevant pairs of polycyclic heteroaromatic amines, that is, amino-3-Me-naphthalene, IQ, 3-Me PhIP, and PhIP, obtained by B3LYP/6-31+G* calculations. As is seen, all 12 focused compounds with the anilinic and 2-aminopyridinic cores fall into one 45° straight line, and the heteroaromatic amines of the 1-methyl-1*H*-imidazole-2-amine scaffold form a parallel line, which is about 6.7 kcal/mol below. This suggests that anionic species derived from $ArNH_2$ and ArNHOH are stabilized by the same electron-withdrawing functions and to an equal extent, which clearly implies structural similarity. Figure 13A and B illustrates resonance structures of the anionic species $ArNH^-$ and $ArNHO^-$ derived from **5** and PhIP and stabilized by electron-withdrawing nitrogens in resonance positions. Thus, the role of the anionic stabilization in the overall mutagenic potency of $ArNH_2$ is amplified in the mutagenic pathway because rate-limiting proton abstraction most likely occurs twice, first during the *N*-hydroxylation by CYP1A2 and second during bioconjugation by Phase II enzymes. This could explain the noted dramatic pro-mutagenic

Table 1. Critical Properties of $ArNH_2$ Obtained by Benchmark ab Initio Calculations, in kcal/mol[a]

	MP2/6-311++G(2df,2p)			MP2/6-311+G(d)//B3LYP/6-31(d)		
molecule	N−H Het DE	RAS	ArNH−OH stability	N−H Het DE	RAS	ArNH−OH stability
1	**373.8**	**0**	**−23.7**	**372.8**	**0**	−17.2
2	**376.5**	**−2.7**	**−49.2**	**375.5**	**−2.7**	−42.0
5	**355.8**	**18.0**	**−10.0**	**354.5**	**18.3**	−3.3
9	**350.6**	**23.2**	**3.7**	**348.7**	**24.1**	10.6
10	**366.3**	**7.5**	**−41.8**	**366.1**	**6.7**	−33.8

[a] Molecules are numbered according to Figure 7. N−H Het DE, heterolytic dissociation energy of N−H bond in $ArNH_2$; RAS, relative anionic stability with respect to the anionic stability of aniline; ArNH−OH stability, energy of proton-assisted heterolytic cleavage of N−O bond in hydroxylamines according to eq 3. Bold data match the highest theoretical level reasonably well.

Table 2. Critical Properties of $ArNH_2$ Obtained by Different DFT Levels, in kcal/mol[a]

	B3LYP/6-31(d)			B3LYP/6-31+G(d)			M06-2X/6-31+G(d)		
molecule	N−H Het DE	RAS	ArNH−OH stability	N−H Het DE	RAS	ArNH−OH stability	N−H Het DE	RAS	ArNH−OH stability
1	386.1	**0**	**−24.4**	**373.6**	**0**	−31.3	**372.9**	**0**	−17.6
2	388.0	**−1.9**	**−48.4**	**376.2**	**−2.5**	−55.3	**375.6**	**−2.6**	−42.4
5	364.5	**21.6**	**−9.9**	**353.8**	**19.8**	−16.9	**353.5**	**19.4**	−2.5
9	359.3	**26.8**	**5.1**	**348.9**	**24.7**	−1.6	**348.4**	**24.5**	12.8
10	375.0	**11.1**	**−44.8**	**364.6**	**9.0**	−51.6	**364.7**	**8.2**	−35.6

[a] Molecules are numbered according to Figure 7. N−H Het DE, heterolytic dissociation energy of N−H bond in $ArNH_2$; RAS, relative anionic stability with respect to the anionic stability of aniline; ArNH−OH stability, energy of proton-assisted heterolytic cleavage of N−O bond in hydroxylamines according to eq 3. Bold data match the highest theoretical level reasonably well.

Table 3. Absolute and Relative Energies of Heterolytic Cleavage of Indicated Bonds in Critical States of the Oxidant along the Mutagenicity Pathway Obtained at Different Levels of Theory in kcal/mol[a]

	B3LYP/6-31G(d)		B3LYP/6-31+G(d)//B3LYP/6-31G(d)		M06-2X/6-31+G(d)//B3LYP/6-31G(d)		MP2/6-311+G(d)//B3LYP/6-31G(d)	
bond	HetDE	relative HetDE	HetDE	relative HetDE	HetDE	relative HetDE	HetDE	relative HetDE
(P)OO−H	435.7	**49.6**	425.1	**52.1**	426.0	**52.3**	428.0	**55.2**
(P)O−OH	463.9		457.9		465.3		499.8	
(P)O(H)O−H	362.9	**−23.2**	352.2	**−20.8**	355.7	**−18.0**	354.8	**−18.0**
(P)O(H)—OH	335.3		332.1		330.5		325.1	

[a] These results were obtained by all-electron calculations using Gaussian 09. (P) stands for methylthiolate-ligated iron(III) porphyrin. Het DE, heterolytic bond dissociation energy of the indicated bond of the oxidant; relative het DE, relative heterolytic bond dissociation energy of the indicated bond of the oxidant with respect to that of aniline. Bold data match the highest theoretical level reasonably well.

effects of electron-withdrawing functions in the resonance positions of $ArNH_2$.[13]

Reflections of the selective disruption of one of the pro-mutagenic factors, which would be more interesting for practical purposes, can be found as well. Disruption of the primary factor, binding affinity of aromatic amines in the CYP1A2 catalytic cavity in the productive binding mode, has to prevent mutagenicity of aromatic amines regardless of the stability of their anionic or cationic forms. Indeed, it is noticed that bulky nonplanar substituents of any chemical nature placed in any position of anilines keep them mutagenicity free and simultaneously make them incompatible with the planar substrate cavity of CYP1A2.[79] Figure 14A gives 20 examples for such structures. One more case of the protective substitution pattern is shown in Figure 2. As is seen, 4-fluoro-3-trifluoromethyl-aniline is Ames negative, even though its anionic and cationic forms are sufficiently stable to make the close analogue, 4-fluoroaniline **3**, and the corresponding nitroarene, 1-fluoro-4-nitro-2-(3-fluoromethyl)benzene (Figure 2), Ames positive. Consistent with experimental results presented in Figure 14A, the bulky *m*-CF_3 group does not allow this aromatic amine to bind to CYP1A2 in the productive binding mode. Another reflection of the effects of shape complementarity of polycyclic $ArNH_2$ and substrate cavity in CYP1A2 is the noticed difference in mutagenic potency caused by different location of the exocyclic NH_2 group with respect to the long axis of the molecule in amino-carbolines.[33] Consistent with a narrow and elongated shape of the substrate cavity in CYP1A2 directed toward the catalytic center,[79] location of NH_2 close to the long axis of polycyclic $ArNH_2$ was found to be associated with higher mutagenic potency. Similarly, the location of NH_2 in 2-naphthylamine close to the long axis of the molecule makes it mutagenic, whereas the lateral NH_2 in 1-naphthylamine reduces its mutagenicity.[113]

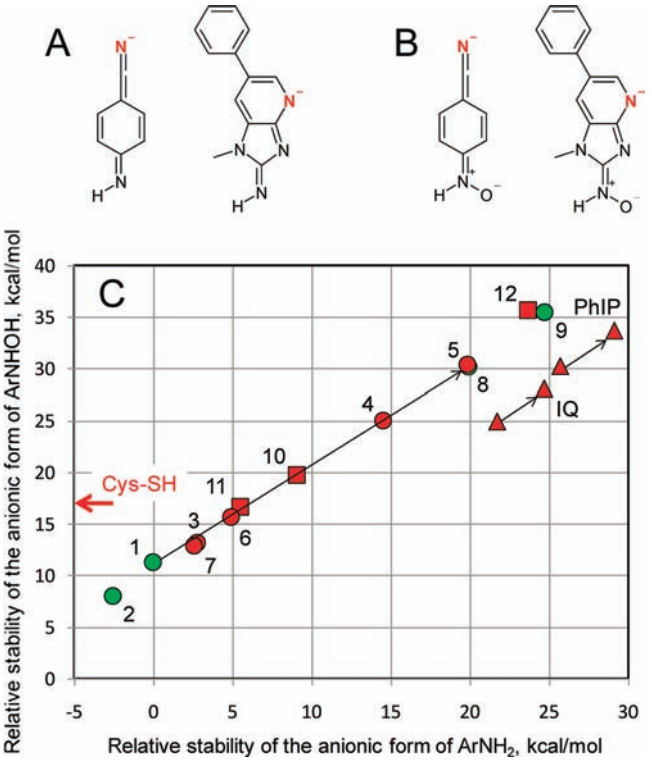

Figure 13. Structural similarity of the anionic forms of $ArNH_2$ and ArNHOH. (A) Resonance structures of anionic forms of **5** and PhIP; (B) resonance structures of anionic forms of hydroxylamines derived from **5** and PhIP. Nitrogen atoms, which stabilize these resonance structures, are highlighted in red. (C) The plot of relative stabilities of the anionic forms of $ArNH_2$ and ArNHOH obtained by DFT calculations at the B3LYP/6-31+G* level of theory for the focused set (Figure 7) and four polycyclic heteroaromatic amines. Mutagenic and nonmutagenic compounds are shown in red and green, respectively. Circles, squares, and triangles signify monocyclic, bicyclic, and tricyclic $ArNH_2$. Stabilization energies of the anionic forms are shown in both axes with respect to the predicted anilinic anion stability, which is −373.6 kcal/mol. The 45° arrows show the effects of electron-withdrawing functions in the resonance positions on the anionic stability. Relative heterolytic S−H bond dissociation energy of cysteine predicted at the same level of theory is indicated by the red arrow.

Specific disruption of the initial proton abstraction event in CYP1A2 has to hinder metabolic activation of aromatic amines to hydroxylamines, regardless of the other two factors. Apart from the known pro-mutagenic effects of electron-withdrawing groups and pyridine-like nitrogens in the food-derived heterocyclic $ArNH_2$,[13,33,60] and the mentioned inability of π-electron donating group OCH_3 in the para position of aniline to form indisputably mutagenic $ArNH_2$ in standard TA98/TA100 strains,[105,106] protective effects of acidic groups suggest an additional argument that this disruption is possible (Figure 14C). The addition of a sulfonic acid moiety to 4-aminobiphenyl **10** and benzidine **11** has been shown to reduce their mutagenicity and carcinogenicity.[114,115] Our model suggests a new explanation for the protective effect of negatively charged groups, that is, preventing proton abstraction in CYP1A2. Indeed, according to B3LYP/6-31G* calculations, energy required for proton abstraction from NH_2 groups of $ArNH_2$ that are already negatively charged is about 100 kcal/mol higher than that from neutral $ArNH_2$ (data not shown).

Preventing the initial proton abstraction by stabilizing the N−H bond of neutral $ArNH_2$ by π-electron -donating groups is not recommended because of possible rewiring of the metabolic activation route in CYP1A2 toward the formation of hydroperoxy radical (Figure 10). In this respect, it is worth comparing two carcinogenic compounds, 4-aminobiphenyl **10** and benzidine **11**. Both compounds are known to be mutagenic and have intrinsic propensities to cause oxidative stress.[43,44] The former compound is more mutagenic in the TA98 tester strain, which is sensitive to mutations caused by DNA adducts (according to our in-house data, the lowest Ames positive doses differ by 100 times, and maximum mutagenic response by 4.2 times), but the latter exhibits higher pro-oxidant propensity.[43] This is in line with the predicted role of the π-electron donating group NH_2 in **11** and concomitant resonance destabilization of its anionic form in rewiring the metabolic transformations in CYP1A2 toward the production of ROS (Figure 10). It is interesting to add that *N*-acetylation of one of the amine groups of **11**, which removes its π-electron-donating capacity, has been found to facilitate the P450-mediated *N*-hydroxylation of the nonacetylated NH_2 group.[6] Analysis of scarce publications on monocyclic $ArNH_2$ that generate free radicals and cause oxidative stress during their metabolism allowed us to find two anilinic compounds, that is, DMPD[116] and *o*-anisidine.[43,117] These $ArNH_2$ have π-electron-donating groups located in resonance positions, *p*-$N(CH_3)_2$ and *o*-OCH_3, respectively, consistent with the obtained results (Figures 10 and 11).

Destabilization of nitrenium ions by electron-withdrawing groups in resonance positions of $ArNH_2$ as an approach to reducing their mutagenic potency is known,[31,50,60] but practical applications of this method to completely obliterate mutagenicity are likely hindered by the simultaneous pro-mutagenic stabilization of the anionic form (Figure 8). In this Article, we demonstrate that at least two electron-withdrawing groups are normally required to disrupt factor F3 and thereby override the pro-mutagenic effects of factor F2 even in monocyclic $ArNH_2$. Figure 14B gives seven Ames negative compounds, in which the factor F3 is sufficiently disrupted by electron-withdrawing groups to make reaction 3 endothermic. There is only one monocyclic $ArNH_2$, 4-aminopyridine (Figure 14B), in which one electron-withdrawing group, pyridine N in the para position, is sufficient to make reaction 3 endothermic. In polycyclic $ArNH_2$, nitrenium ions are generally more stable (e.g., see Figure 8B), which makes the factor F3 alone insufficient to remove mutagenicity, contrary to current opinion.[55−57]

Rational design of mutagenicity free $ArNH_2$ has to start from what is to be avoided: quasi-planar aromatic systems with two or more aromatic rings, similar to known carcinogenic compounds like 2-aminofluorene, 4-aminobiphenyl, 2-naphthylamine, benzidine, *o*-tolidine, or the food-derived heterocyclic amines. Apart from having especially stable anionic and nitrenium forms, polycyclic $ArNH_2$ that have their long axis passing close to the NH_2 group fit to the CYP1A2 cavity particularly well, and, as such, will likely be highly mutagenic. On the other hand, polycyclic $ArNH_2$ with NH_2 group located roughly perpendicular to the long axis, similar to weakly mutagenic 1-naphthylamine,[113] could be either nonmutagenic or made nonmutagenic after minor structural alterations. On the basis of our results, we propose that the best strategy to design mutagenicity free $ArNH_2$ is to make the binding mode required for effective proton abstraction in CYP1A2 inconsistent with the planar and elongated shape of the substrate cavity of the enzyme. Sterical clashes

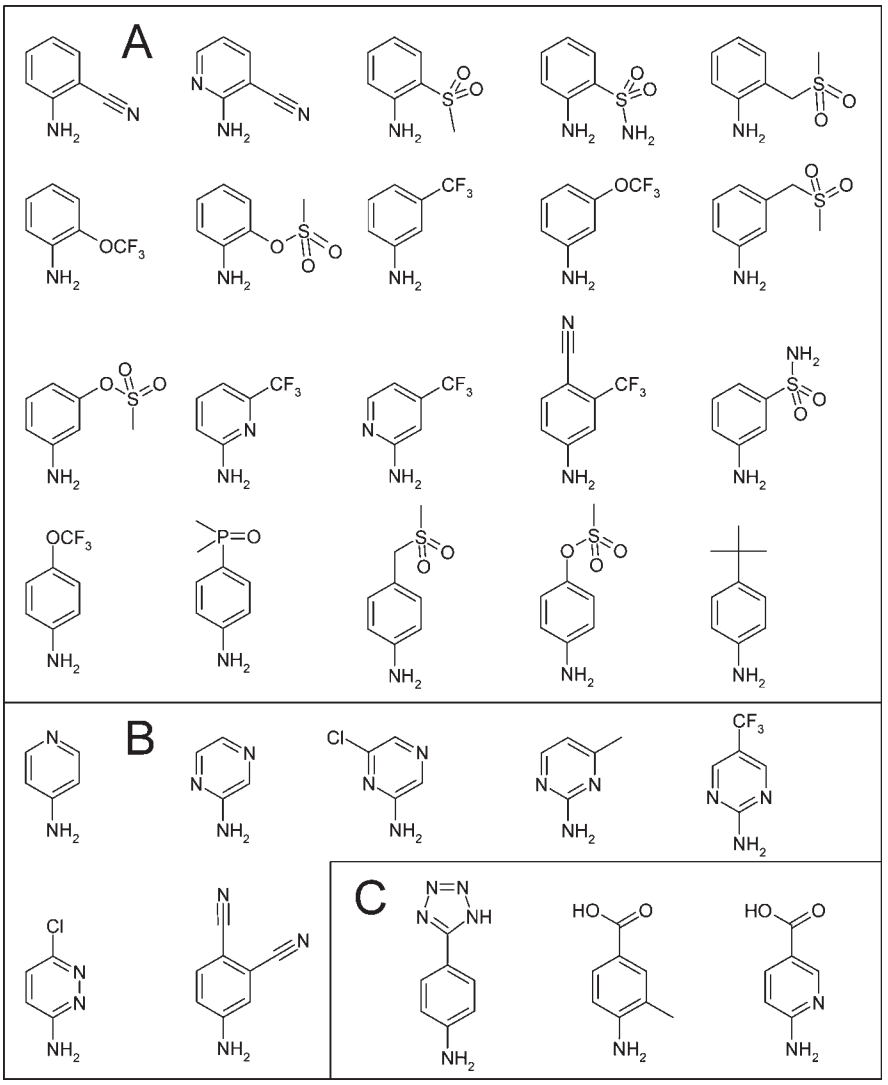

Figure 14. Examples of mutagenicity-free aromatic amines as confirmed in Ames assays in TA98/TA100 strains. Bulky groups, especially in ortho or meta positions, regardless of their chemical nature make aromatic amines given in section A incompatible with the substrate cavity of CYP1A2. Electron-withdrawing groups in anilines illustrated in section B stabilize hydroxylamines and their bioconjugates to prevent proton-assisted hydrolytic dissociation to DNA-reactive nitrenium ions. An acidic group in para position prevents proton abstraction from NH_2 group of anilines in section C by the ferric peroxo intermediate of CYP1A2.

with the substrate cavity can be engineered by making $ArNH_2$ nonplanar either by adding nonplanar functions or by making the conformation of the entire molecule essentially nonplanar. Another strategy is to change the shape of the molecule by making it wider, rather than longer. According to the internal AstraZeneca Ames mutagenicity database (Figure 4) and X-ray crystallographic data,[79] the preferred positions of protective functions in substituted anilines are ortho and meta, with the para position being also possible but usually requiring more drastic solutions. Our observations presented in Figure 14A indicate that the *o*-CN group prevents mutagenicity of compounds with anilinic and 2-aminopyridinic scaffolds, whereas CF_3 group is reliable only in meta position. Bulkier nonplanar groups, like OCF_3, SO_2CH_3, OSO_2CH_3, $CH_2SO_2CH_3$, SO_2NH_2, $SO_2N(CH_3)_2$, and *t*-Bu, are effective in all positions. In addition, an acidic group could be added in the para position, where it cannot be wired to the proton delivery systems of the enzyme and be protonated to facilitate proton abstraction from the NH_2 group.

■ CONCLUSIONS

In this study, we suggest a heterolytic mechanism of metabolic activation of aromatic and heteroaromatic amines by CYP1A2 enzyme, which explains the main features of their structure −mutagenicity relationships. Thus, on the basis of the observed experimental SAR, geometric considerations, and calculated heterolytic bond dissociation energies, we propose a mechanism for *N*-hydroxylation by CYP1A2 different from the established mechanism for *C*-hydroxylation. While beyond the scope of this study, we note that key intermediates of the proposed mechanism should be possible to observe experimentally; detailed kinetic and spectroscopic studies would be important to fully understand the mechanism and reaction rates. The rate-limiting step of the mechanism is likely to be proton abstraction from aromatic amine bound to the CYP1A2 substrate cavity by the dianionic ferric peroxo intermediate. Accordingly, stabilization of the anionic forms of arylamines by electron-withdrawing groups facilitates their metabolic activation by CYP1A2. As a part of

this mechanism, a possibility of formation of hydroperoxy radical in CYP1A2 triggered by binding of aromatic amines with π-electron-donating groups in resonance positions is noted. This is consistent with earlier observations indicating that binding of such molecules to the CYP1A2 catalytic site causes oxidative stress. In the productive binding mode, the NH_2 group of aromatic amine is squeezed between the distal oxygen atom of the $(CYP1A2)Fe(III)-OO^-$ peroxo moiety and OH group of residue T-124 of human CYP1A2. Results suggest that there are three factors that make aromatic amines mutagenic: (i) high affinity of the productive binding mode in CYP1A2 prior to proton abstraction, (ii) ease of proton abstraction from the NH_2 group, and (iii) exothermicity of proton-assisted dissociation of hydroxylamine. The role of the resonance stabilization of the anionic form of aromatic amines in the overall mutagenic potency is likely further amplified by the following transient proton abstraction from hydroxylamines during bioconjugation in Phase II enzymes. The attained structure–based understanding of the mutagenic potency of aromatic amines and chemistry of the metabolic activation enable us to devise a potential design strategy of nonmutagenic aromatic amine fragments for drug discovery programs. We suggest three ways to design mutagenicity free aromatic amines: (i) by destabilizing productive binding mode of aromatic amines in CYP1A2 through disrupting geometric compatibility with the substrate cavity, for example, by making the aromatic amines essentially nonplanar or by adding bulky groups, preferably in ortho or meta positions; (ii) by strongly stabilizing the N–O bonds of monocyclic hydroxylamines with electron-withdrawing groups to prevent their hydrolytic dissociation; and (iii) by adding acidic functions in the para position.

■ ASSOCIATED CONTENT

Supporting Information. Figures 1S and 2S, and energies and energy-optimized geometries of compounds and complexes discussed in this Article. This material is available free of charge via the Internet at http://pubs.acs.org.

■ AUTHOR INFORMATION

Corresponding Author
igor.shamovsky@astrazeneca.com

■ ACKNOWLEDGMENT

Fruitful discussions with Andrew G. Leach, Frank Narjes, Steve Swallow, and Andrew Teasdale are highly appreciated. Niklas Blomberg and Scott Boyer are acknowledged for both discussions and reviewing the paper. We would like to express our sincere gratitude to all personnel of Information Technology and High-performance Computing Departments of AstraZeneca R&D Mölndal, and in particular Roger Andersson, Martin Budsjö, and Lisa Hamberg. High professionalism and positive attitude of these three individuals made the presented computational studies possible.

■ REFERENCES

(1) Snyder, R. D. *Environ. Mol. Mutagen.* **2009**, *50*, 435–450.
(2) Mizra, A.; Desai, R.; Reynisson, J. *Eur. J. Med. Chem.* **2009**, *44*, 5006–5011.
(3) Hillebrecht, A.; Muster, W.; Brigo, A.; Kansy, M.; Weiser, T.; Singer, T. *Chem. Res. Toxicol.* **2011**, *24*, 843–854.
(4) Rehn, L. *Arch. Klin. Chir.* **1895**, *50*, 588–600.
(5) Case, R. A. M.; Hosker, M.-E.; McDonald, D. B.; Pearson, J. T. *Br. J. Ind. Med.* **1954**, *11*, 213–216.
(6) Turesky, R. J. In *The Chemical Biology of DNA Damage*; Geacintov, N. E., Broyde, S., Eds.; Wiley-VCH Verlag: Weinheim, 2010; pp 157–183.
(7) Miller, J. A.; Miller, E. C. *Environ. Health Perspect.* **1983**, *49*, 3–12.
(8) Garner, R. C.; Martin, C. N.; Clayson, D. B. In *Chemical Carcinogenesis*, 2nd ed.; Searle, C. E., Ed.; American Chemical Society: Washington, DC, 1984; Vol. 1, pp 175–276.
(9) Wakabayashi, K.; Nagao, M.; Esumi, H.; Sugimura, T. *Cancer Res.* **1992**, *52*, 2092s–2098s.
(10) Chung, K.-T.; Kirkovsky, L.; Kirkovsky, A.; Purcell, W. P. *Mutat. Res.* **1997**, *387*, 1–16.
(11) Patel, D. J.; Mao, B.; Gu, Z.; Hingerty, B. E.; Gorin, A.; Basu, A. K.; Broyde, S. *Chem. Res. Toxicol.* **1998**, *11*, 391–407.
(12) Felton, J. S.; Knize, M. G.; Bennett, L. M.; Malfatti, M. A.; Colvin, M. E.; Kulp, K. S. *Toxicology* **2004**, *198*, 135–145.
(13) Felton, J. S.; Knize, M. G.; Wu, R. W.; Colvin, M. E.; Hatch, F. T.; Malfatti, M. A. *Mutat. Res.* **2007**, *616*, 90–94.
(14) Beland, F. A.; Kadbular, F. F. Cancinogenesis and Mutagenesis. In *Handbook of Experimental Pathology*; Cooper, C. S., Glover, P. L., Eds.; Springer: Heidelberg, 1990; Vol. 94, pp 267–325.
(15) Turesky, R. J.; Lang, N. P.; Butler, M. A.; Teitel, C. H.; Kadbular, F. F. *Carcinogenesis* **1991**, *12*, 1839–1845.
(16) Turesky, R. J.; Constable, A.; Richoz, J.; Varga, N.; Markovic, J.; Martin, M. V.; Guengerich, F. P. *Chem. Res. Toxicol.* **1998**, *11*, 925–936.
(17) Kerdar, R. S.; Dehner, D.; Wild, D. *Toxicol. Lett.* **1993**, *67*, 73–85.
(18) Guengerich, F. P.; Hemphreys, W. G.; Yun, C. H.; Hammons, G. J.; Kadlubar, F. F.; Seto, Y.; Okazaki, O.; Martin, M. V. *Princess Takamatsu Symp.* **1995**, *23*, 78–84.
(19) Colvin, M. E.; Hatch, F. T.; Felton, J. S. *Mutat. Res.* **1998**, *400*, 479–492.
(20) Luch, A. *Nat. Rev.* **2005**, *5*, 113–125.
(21) Tsuneoka, Y.; Dalton, T. P.; Miller, M. L.; Clay, C. D.; Shertzer, H. G.; Talaska, G.; Medvedovic, M.; Nebert, D. W. *J. Natl. Cancer Inst.* **2003**, *95*, 1227–1237.
(22) Kim, D.; Guengerich, F. P. *Annu. Rev. Pharmacol. Toxicol.* **2005**, *45*, 27–49.
(23) Butler, M. A.; Guengerich, F. P.; Kadbular, F. F. *Cancer Res.* **1989**, *49*, 25–31.
(24) Eaton, D. L.; Gallagher, E. P.; Bammler, T. K.; Kunze, K. L. *Pharmacogenetics* **1995**, *5*, 259–274.
(25) Weisburger, J. H. *Mutat. Res.* **2002**, *506–507*, 9–20.
(26) Guengerich, F. P. In *Cytochrome P450: Structure, Mechanism and Biochemistry*, 3rd ed.; Ortiz de Montellano, P. R., Ed.; Kluwer Academic/Plenum Publishers: New York, 2005; pp 377–530.
(27) Hoffmann, G. R.; Fuchs, R. P. P. *Chem. Res. Toxicol.* **1997**, *10*, 347–359.
(28) Guengerich, F. P.; Rarikh, A.; Yun, C.-H.; Kim, D.; Nakamura, K.; Notley, L. M.; Gillam, E. M. J. *Drug Metab. Rev.* **2000**, *32*, 267–281.
(29) Kulkarni, S. A.; Moir, D.; Zhu, J. *SAR QSAR Environ. Res.* **2007**, *18*, 459–514.
(30) Grant, D. M.; Josephy, P. D.; Lord, H. L.; Morrison, L. D. *Cancer Res.* **1992**, *52*, 3961–3964.
(31) Novak, M.; Rajagopal, S.; Xu, L.; Kazerani, S.; Toth, K.; Brooks, M.; Nguyen, T.-M. *J. Phys. Org. Chem.* **2004**, *17*, 615–624.
(32) Cho, B. In *The Chemical Biology of DNA Damage*; Geacintov, N. E., Broyde, S., Eds.; Wiley-VCH Verlag: Weinheim, 2010; pp 217–238.
(33) Hatch, F. T.; Knize, M. G.; Felton, J. S. *Environ. Mol. Mutagen.* **1991**, *17*, 4–19.
(34) Mao, B.; Hingerty, B. E.; Broyde, S.; Patel, D. J. *Biochemistry* **1998**, *37*, 81–94.
(35) Chiapperino, D.; McIlroy, S.; Falvey, D. E. *J. Am. Chem. Soc.* **2002**, *124*, 3567–3577.
(36) Dutta, S.; Li, Y.; Johnson, D.; Dzantiev, L.; Richardson, C. C.; Romano, L. J.; Ellenberger, T. *Proc. Natl. Acad. Sci. U.S.A.* **2004**, *101*, 16186–16191.
(37) Loeb, L.; Harris, C. C. *Cancer Res.* **2008**, *68*, 6863–6872.

(38) Beland, F. A.; Melchior, W. B., Jr.; Mourato, L. L. G.; Santos, M. A.; Marques, M. M. *Mutat. Res.* **1997**, *376*, 13–19.
(39) Hatch, F. T.; Knize, M. G.; Colvin, M. E. *Environ. Mol. Mutagen.* **2001**, *38*, 268–291.
(40) Kriek, E. *Cancer Res.* **1972**, *32*, 2042–2048.
(41) Parks, J. M.; Ford, G. P.; Cramer, C. J. *J. Org. Chem.* **2001**, *66*, 8997–9004.
(42) Hirano, T.; Higashi, K.; Sakai, A.; Tsurudome, Y.; Ootsuyama, Y.; Kido, R.; Kasai, H. *Jpn. J. Cancer Res.* **2000**, *91*, 681–685.
(43) Siraki, A. G.; Chan, T. S.; Galati, G.; Teng, S.; O'Brien, P. J. *Drug Metab. Rev.* **2002**, *34*, 549–564.
(44) Makena, P. S.; Chung, K.-T. *Environ. Mol. Mutagen.* **2007**, *48*, 404–413.
(45) Blair, I. A. *J. Biol. Chem.* **2008**, *283*, 15545–15549.
(46) Shafirovich, V.; Geacintov, N. E. In *The Chemical Biology of DNA Damage*; Geacintov, N. E., Broyde, S., Eds.; Wiley-VCH Verlag: Weinheim, 2010; pp 82−104.
(47) Knutson, C. G.; Marnett, L. J. In *The Chemical Biology of DNA Damage*; Geacintov, N. E., Broyde, S., Eds.; Wiley-VCH Verlag: Weinheim, 2010; pp 105−129.
(48) Shahin, M. M. *Mutat. Res.* **1987**, *181*, 243–256.
(49) Sabbioni, G.; Wild, D. *Carcinogenesis* **1992**, *13*, 709–713.
(50) Ford, G. P.; Griffin, G. R. *Chem.-Biol. Interact.* **1992**, *81*, 19–33.
(51) Ford, G. P.; Herman, P. S. *Chem.-Biol. Interact.* **1992**, *81*, 1–18.
(52) Debnath, A. K.; Debnath, G.; Shusterman, A. J.; Hansch, C. *Environ. Mol. Mutagen.* **1992**, *19*, 37–52.
(53) Benigni, R.; Andreoli, C.; Giuliani, A. *Environ. Mol. Mutagen.* **1994**, *24*, 208–219.
(54) Benigni, R.; Giuliani, A.; Franke, R.; Gruska, A. *Chem. Rev.* **2000**, *100*, 3697–3714.
(55) Leach, A. G.; Cann, R.; Tomasi, S. *Chem. Commun* **2009**, 1094–1096.
(56) Bentzien, J.; Hickey, E. R.; Kemper, R. A.; Brewer, M. L.; Dyekjar, J. D.; East, S. P.; Whittaker, M. *J. Chem. Inf. Model.* **2010**, *50*, 274–297.
(57) McCarren, P.; Bebernitz, G. R.; Gedeck, P.; Glowienke, S.; Grondine, M. S.; Kirman, L. C.; Klickstein, J.; Schuster, H. F.; Whitehead, L. *Bioorg. Med. Chem.* **2011**, *19*, 3173–3182.
(58) Kadbular, F. F.; Beland, F. A. In *Polycyclic Hydrocarbons and Carcinogenesis*; ACS Symposium Series 283; Harvey, R. G., Ed.; American Chemical Society: Washington, DC, 1985; pp 341−370.
(59) Wild, D.; Dirr, A. *Mutagenesis* **1989**, *4*, 446–452.
(60) Borosky, G. L. *Chem. Res. Toxicol.* **2007**, *20*, 171–180.
(61) Hatch, F. T.; Colvin, M. E.; Seidl, E. T. *Environ. Mol. Mutagen.* **1996**, *27*, 314–330.
(62) Sabbioni, G. *Environ. Health Perspect.* **1994**, *102*, 61–67.
(63) Purohit, V.; Basu, A. K. *Chem. Res. Toxicol.* **2000**, *13*, 673–692.
(64) Sasaki, J. C.; Fellers, R. S.; Colvin, M. E. *Mutat. Res.* **2002**, *506−507*, 79–89.
(65) Guengerich, F. P. *Chem. Res. Toxicol.* **2001**, *14*, 611–650.
(66) Filatov, M.; Harris, N.; Shaik, S. *Angew. Chem., Int. Ed.* **1999**, *38*, 3510–3512.
(67) Shaik, S.; Cohen, S.; Wang, Y.; Chen, H.; Kumar, D.; Thiel, W. *Chem. Rev.* **2010**, *110*, 949–1017.
(68) Rittle, J.; Green, M. T. *Science* **2010**, *330*, 933–937.
(69) Franke, R.; Gruska, A.; Giuliani, A.; Benigni, R. *Carcinogenesis* **2001**, *22*, 1561–1571.
(70) Sushko, I.; et al. *J. Chem. Inf. Model.* **2010**, *50*, 2094–2111.
(71) Muratov, E.; et al. The 241st ACS National Meeting, Anaheim, CA, 2011; CINF-58.
(72) Becke, A. *J. Chem. Phys.* **1993**, *98*, 5648–5652.
(73) Meunier, B.; de Visser, S. P.; Shaik, S. *Chem. Rev.* **2004**, *104*, 3947–3980.
(74) Cundari, T. R.; Stevens, W. J. *J. Chem. Phys.* **1993**, *98*, 5555–5565.
(75) Siegbahn, E. M. *J. Biol. Inorg. Chem.* **2006**, *11*, 695–701.
(76) Clark, T.; Chandrasekhar, J.; Spitznagel, G. W.; Schleyer, P. v. R. *J. Comput. Chem.* **1983**, *4*, 294–301.
(77) Zhao, Y.; Truhlar, D. G. *J. Phys. Chem.* **2006**, *110*, 5121–5129.
(78) Møller, C.; Plesset, M. S. *Phys. Rev.* **1934**, *46*, 618–622.
(79) Sansen, S.; Yano, J. K.; Reynald, R. L.; Schoch, G. A.; Griffin, K. J.; Stout, C. D.; Johnson, E. F. *J. Biol. Chem.* **2007**, *282*, 14348–14355.
(80) Frisch, M. J.; et al. *Gaussian 09*, revision B.01; Gaussian, Inc.: Wallingford, CT, 2010.
(81) Maron, D. M.; Ames, B. N. *Mutat. Res.* **1983**, *113*, 173–215.
(82) Mortelmans, K.; Zeiger, E. *Mutat. Res.* **2000**, *455*, 29–60.
(83) Sugimura, T. *Environ. Health Perspect.* **1998**, *106*, A522–A523.
(84) Ohnishi, S.; Murata, M.; Oikawa, S.; Totsuka, Y.; Takamura, T.; Wakabayashi, K.; Kawanishi, S. *Mutat. Res.* **2001**, *494*, 63–72.
(85) Denisov, I. G.; Makris, T. M.; Sligar, S. G.; Schlichting, I. *Chem. Rev.* **2005**, *105*, 2253–2277.
(86) Sono, M.; Roach, M. P.; Coulter, E. D.; Dawson, J. H. *Chem. Rev.* **1996**, *96*, 2841–2887.
(87) Toy, P. H.; Newcomb, M.; Coon, M. J.; Vaz, A. D. N. *J. Am. Chem. Soc.* **1998**, *120*, 9718–9719.
(88) Newcomb, M.; Shen, R.; Choi, S.-Y.; Toy, P. H.; Hollenberg, P. F.; Vaz, A. D. N.; Coon, M. J. *J. Am. Chem. Soc.* **2000**, *122*, 2677–2686.
(89) Newcomb, M.; Toy, P. H. *Acc. Chem. Res.* **2000**, *33*, 449–455.
(90) Volz, T. J.; Rock, D. A.; Jones, J. P. *J. Am. Chem. Soc.* **2002**, *124*, 9724–9725.
(91) Wang, A.; Savas, U.; Stout, C. D.; Johnson, E. F. *J. Biol. Chem.* **2011**, *286*, 5736–5743.
(92) White, R. E. *Pharmacol. Ther.* **1991**, *49*, 21–42.
(93) Darbyshire, J. F.; Iyer, K. R.; Grogan, J.; Korzekwa, K. R.; Trager, W. F. *Drug Metab. Dispos.* **1996**, *24*, 1038–1045.
(94) Sarabia, S. F.; Zhu, B. T.; Kurosawa, T.; Tohma, M.; Liehr, J. G. *Chem. Res. Toxicol.* **1997**, *10*, 767–771.
(95) Rydberg, P.; Ryde, U.; Olsen, L. *J. Phys. Chem. A* **2008**, *112*, 13058–13065.
(96) Shvedova, A. A.; Kommineni, C.; Jeffries, B. A.; Castranova, V.; Tyurina, Y. Y.; Tyurin, V. A.; Serbinova, E. A.; Fabisiak, J. P.; Kagan, V. E. *J. Invest. Dermatol.* **2000**, *114*, 354–364.
(97) Ingold, K. U.; Wright, J. S. *J. Chem. Educ.* **2000**, *77*, 1062–1064.
(98) Bach, R. D.; Ayala, P. Y.; Schlegel, H. B. *J. Am. Chem. Soc.* **1996**, *118*, 12758–12765.
(99) Meunier, B.; Bernadou, J. *Struct. Bonding* **2000**, *97*, 1–35.
(100) Groenhof, A. R.; Ehlers, A. W.; Lammertsma, K. *J. Am. Chem. Soc.* **2007**, *129*, 6204–6209.
(101) Kaila, V. R. I.; Verkhovsky, M. I.; Wikström, M. *Chem. Rev.* **2010**, *110*, 7062–7081.
(102) Guengerich, F. P.; Miller, G. P.; Hanna, I. H.; Sato, H.; Martin, M. V. *J. Biol. Chem.* **2002**, *277*, 33711–33719.
(103) Krishtal, A.; Vanommeslaeghe, K.; Olatz, A.; Veszprémi, T.; van Alsenoy, C.; Geerlings, P. *J. Chem. Phys.* **2009**, *130*, 174101–174108.
(104) Zimmer, D.; Mazurek, J.; Petzold, G.; Bhuyan, B. K. *Mutat. Res.* **1980**, *77*, 317–326.
(105) Klopman, G.; Frierson, M. R.; Rosenkranz, H. S. *Environ. Mutagen.* **1985**, *7*, 625–644.
(106) Thompson, D. C.; Josephy, P. D.; Chu, J. W. K.; Eling, T. E. *Mutat. Res.* **1992**, *279*, 83–89.
(107) Trieff, N. M.; Biagi, G. L.; Ramanujam, V. M. S.; Connor, T. H.; Cantelli-Forti, G.; Guerra, M. C.; Bunce, H., III; Legator, M. S. *J. Mol. Toxicol.* **1989**, *2*, 53–65.
(108) Campbell, J. J.; Glover, S. A.; Hammond, G. P.; Rowbottom, C. A. *J. Chem. Soc., Perkin Trans. 2* **1991**, 2067–2079.
(109) Lau, E. Y.; Felton, J. S.; Lightstone, F. C. *Chem. Res. Toxicol.* **2006**, *19*, 1182–1190.
(110) Wu, H.; Dombrovsky, L.; Tempel, W.; Martin, F.; Loppnau, P.; Goodfellow, G. H.; Grant, D. M.; Plotnikov, A. N. *J. Biol. Chem.* **2007**, *282*, 30189–30197.
(111) Qiao, Q.-A.; Yang, C.; Qu, R.; Jin, Y.; Wang, M.; Zhang, Z.; Xu, Q.; Yu, Z. *Biophys. Chem.* **2006**, *122*, 215–220.
(112) Grant, D. M. *Curr. Drug Metab.* **2008**, *9*, 465–470.
(113) Oglesby, L. A.; Hix, C.; Snow, L.; MacNair, P.; Seig, M.; Langenbach, R. *Cancer Res.* **1983**, *43*, 5194–5199.

(114) Ashby, J.; Paton, D.; Lefevre, P. A.; Styles, J. A.; Rose, F. L. *Carcinogenesis* **1982**, *3*, 1277–1282.
(115) Chung, K.-T.; Chen, S.-C.; Claxton, L. D. *Mutat. Res.* **2006**, *612*, 58–76.
(116) Dimethyl-4-phenylenediamine (DMPD) was shown to generate free radicals: Ben Mansour, H.; Barillier, D.; Corroler, D.; Ghedira, K.; Chekir-Ghedira, L.; Mosrati, R. *Environ. Toxicol. Chem.* **2009**, *28*, 489–495.
(117) Brennan, R. J.; Schiestl, R. H. *Mutat. Res.* **1999**, *430*, 37–45.